MOX–Report No. 52/2014

Isogeometric analysis and proper orthogonal decomposition for parabolic problems

Dede , L..; Quarteroni, A.; S. Zhu, S.

MOX, Dipartimento di Matematica "F. Brioschi"
Politecnico di Milano, Via Bonardi 9 - 20133 Milano (Italy)

mox@mate.polimi.it http://mox.polimi.it

Noname manuscript No.
(will be inserted by the editor)

Isogeometric analysis and proper orthogonal decomposition for parabolic problems

Luca Dedè · Alfio Quarteroni · Shengfeng Zhu

Received: date / Accepted: date

Abstract We investigate the combination of Isogeometric Analysis (IGA) and proper orthogonal decomposition (POD) based on the Galerkin method for model order reduction of linear parabolic partial differential equations. For the proposed fully discrete scheme, the associated numerical error features three components due to spatial discretization by IGA, time discertization with the θ-scheme, and eigenvalue truncation by POD. First, we prove *a priori* error estimates of the spatial IGA semi-discrete scheme. Then, we show stability and prove *a priori* error estimates of the space-time discrete scheme and the fully discrete IGA-θ-POD Galerkin scheme. Numerical tests are provided to show efficiency and accuracy of NURBS-based IGA for model order reduction in comparison with standard finite element-based POD techniques.

Mathematics Subject Classification (2000) 35K20 · 65M12 · 65M15 · 65M60

1 Introduction

Proper orthogonal decomposition (POD) is a powerful model order reduction technique widely used nowadays in Computational Sciences and Engineering (see e.g. [5,21,36,37, 45]). The method is also used under different names and formulations in other fields ([21]), e.g. principle component analysis in statistics and Karhunen-Loève expansion in stochastic

The third author was financially supported in part by the National Natural Science Foundation of China under grants No. 11201153 and 11371145 and a postdoctoral scholarship from China Scholarship Council.

L. Dedè · A. Quarteroni · S. Zhu
CMCS-Chair of Modeling and Scientific Computing, MATHICSE-Mathematics Institute of Computational Science and Engineering, EPFL-École Polytechnique Fédérale de Lausanne, Station 8, CH-1015, Lausanne, Switzerland
E-mail: luca.dede@epfl.ch; alfio.quarteroni@epfl.ch; shengfeng.zhu@epfl.ch

A. Quarteroni
MOX-Modeling and Scientific Computing, Department of Mathematics, Politecnico di Milano, Piazza L. da Vinci 32, I-20133, Milano, Italy (on leave)

S. Zhu(✉)
Department of Mathematics, East China Normal University, Shanghai 200241, PR China
E-mail: sfzhu@math.ecnu.edu.cn

analysis. In computational mechanics, POD techniques have been applied in various Engineering fields, such as the simulation of turbulent flows [5], weather forecast [31], the solution of optimal control problems [26], and, recently, for reduced order modelling of physical and geometry parameterized steady and unsteady partial differential equations (PDEs); see e.g. [8,18,29,34,39,45]. POD-Galerkin methods for time-dependent PDEs usually perform model order reduction of the solution manifolds depending on the time independent variable, which can also be regarded as a one-dimensional parameter for parameterized PDEs. POD techniques have been mainly applied to parabolic PDEs [19,24,27,40] and Navier-Stokes equations [17,28,31].

POD-Galerkin methods were first analyzed by Kunisch and Volkwein under a unified framework for evolution problems including heat and Burgers equations [27] and, later, the Navier-Stokes equations [28]. The *method of snapshots* in POD-Galerkin methods chooses discrete instances in the parameter domain and uses the corresponding field variables (i.e. the snapshots) to obtain a low-dimensional basis [27,44]. The generation of snapshots is the first crucial step in POD-Galerkin reduced modeling of PDEs. For error estimation and generation of the POD basis proposed in [27,28], the snapshots are often assumed to be "exact" regardless of the space discretization, i.e. given by the exact (weak) solutions at discrete time instances. Therefore, the error between the POD-Galerkin solution and the exact solution is composed by only two components due to the time discretization and POD eigenvalue truncation, respectively.

Nevertheless, "exact" snapshots are usually not available in practice and instead "very accurate", but approximate snapshots are considered. These are generally obtained by spatially approximating the PDEs by means of suitable numerical methods. Then, a question arises: how much this approximation influences the POD-Galerkin solution in terms of accuracy? Indeed, the available snapshot instances contain error due to spatial discretization, which should be reliable or accurate enough in order to consider this error negligible. Most of the existing methods of snapshots thus need to compute snapshots numerically by discretization techniques, such as the Finite Element method (FEM) (see e.g. [7,25,27,30,31, 41]) or Finite Volumes [32]. In [24,31], attempts were made to analyze the error associated to the snapshots. As a popular model order reduction technique, POD is usually designed to capture the information contained in the set of snapshots in the sense of least-squares. This does not necessarily implies that the reduced order space spanned by the POD basis performs well in approximating the solution space (or manifold) of the PDE. For example, let us assume that u is an exact solution of a given PDE. Let us denote by u_s and u_r a snapshot and a POD solution, respectively; then, we have in an arbitrary norm $\|\cdot\|$ the following result [18]:

$$\|u-u_r\| \leq \|u-u_s\| + \|u_s-u_r\| \tag{1}$$

by the triangle inequality. In this respect, POD model order reduction deals with the reduction of the error component $\|u_s-u_r\|$ by modal analysis and eigenmodes truncation. Therefore, to make $\|u-u_s\|$ and hence the total norm $\|u-u_r\|$ small, we need good "approximate" snapshots (also called "truth" approximations [44]) to begin with. Motivated by this requirement, in this paper we choose *Isogeometric Analysis* (IGA) [9,22] to obtain our snapshots in place of the standard FEM. The motivation stems from the fact that the geometrical approximation of the computational domain may affect the accuracy of the POD-Galerkin method, especially if only a "small" number of POD basis functions can be practically used in the POD-Galerkin method.

Compared with standard FEM, IGA has shown many advantages especially in facilitating the exact representation of the computational domains described by Non-Uniform

Rational B-spline (NURBS) in the analysis. Nowadays, IGA has been applied successfully in various Engineering fields including structural mechanics, acoustics, computational fluid dynamics, electromagnetism; see e.g. [2,3,6,9,12,14,38,42]. IGA represents a generalization of the *isoparametric* FEM for which NURBS basis functions, the standard in Computer-Aided Design (CAD), are first used for the geometrical representation of the computational domain and then as basis for the finite-dimensional trial spaces of the solution approximating the PDEs. In particular, the global regularity k_{m} of the NURBS basis functions can be enhanced up to $k_{\mathrm{m}} = p-1$, with p denoting the polynomial degree, conversely to the standard C^0-continuous Lagrange basis functions of the FEM. Moreover, besides h- and p- refinements, IGA enjoys a further refinement called *k-refinement*, which allows $k_{\mathrm{m}} = p-1$ continuity of the basis functions for p-degree NURBS. Therefore, besides the geometric advantages, NURBS-based IGA possesses the advantage of yielding highly accurate approximations when using C^{p-1}-continuous basis functions for smooth solutions of the PDEs. Moreover, in eigenvalue problems the regular basis functions are significantly better than their C^0-continuous counterpart in the computation of the spectrum and modal analysis [10,13,23]. This advantage may be significant in the context of the POD-Galerkin method which is based on modal analysis and eigenvalue truncation. For this reason, together with the exactness of the geometrical representation, we believe that the use of IGA with NURBS basis functions which are C^{p-1}-continuous may be significantly beneficial for POD-Galerkin methods both in terms of accuracy and efficiency.

The aim of this paper is to use IGA for the POD-Galerkin method in model order reduction of linear parabolic PDEs. To the best of our knowledge, this is the first study of the combined use of IGA and POD methods. In addition, we unify the analysis of the method of snapshots based on forward Euler, backward Euler, and Crank-Nicolson schemes for the time discretization (e.g. [24,27,28]) into the general framework of the θ-method, for which we propose the IGA-θ-POD Galerkin method; the corresponding stability and convergence properties are also presented. In Section 2, we first introduce the essential formulations of IGA for the spatial discretization of PDEs. Then, the IGA semi-discrete and fully space-time (with the θ-scheme) discrete methods are presented and stability and convergence analysis of these schemes for parabolic PDEs are provided. In Section 3, we recall the POD methods for model order reduction of PDEs with the time parameter. In Section 4, we present the IGA-θ-POD Galerkin scheme and analyze its stability and convergence analysis by carrying out *a priori* error estimates. We compare numerically the IGA-θ-POD Galerkin method with FEM-θ-POD Galerkin method for reduced order modelling of linear parabolic PDEs. We show that the method using IGA is more accurate and efficient than the one based on FEM, which is used widely in the model reduction literature. Conclusions follow.

2 IGA for linear parabolic problems

In this section, we first introduce the unsteady advection-diffusion-reaction model problem. We introduce B-splines and NURBS for the formulation of IGA. Then, we propose the spatial discretization scheme by IGA and time discretization using the θ-scheme. For the spatial semi-discretization scheme, we show *a priori* error estimates; then, we analyze the stability and convergence properties of the full IGA-θ scheme.

2.1 Problem formulations

Let $\Omega \subset \mathbb{R}^d$ ($d \in \mathbb{N}$) be an open and bounded domain with Lipschitz-continuous boundary $\Gamma := \partial\Omega$. We introduce a second order differential operator L given by

$$Lv := -\sum_{i,j=1}^{d} D_i(\tilde{a}_{ij} D_j v) + \sum_{i=1}^{d} \big(D_i(b_i v) + c_i D_i v\big) + a_0 v, \tag{2}$$

where $D_j := \partial/\partial x_j$ is the spatial derivative operator and the coefficients $\tilde{a}_{ij}, b_i, c_i, a_0 \in L^\infty(\Omega)$ for all $i, j = 1, \dots, d$. We assume that L is *elliptic*, i.e. there exists a constant $\tilde{\alpha} > 0$ such that $\sum_{i,j=1}^{d} \tilde{a}_{ij}(x)\xi_i\xi_j \geq \tilde{\alpha}|\xi|^2$ for all $\xi \in \mathbb{R}^d$ and a.e. in Ω. We consider the following linear initial-boundary value parabolic problem ([35])

$$\begin{cases} \dfrac{\partial u}{\partial t} + Lu = f & \text{in } \Omega_T := (0,T) \times \Omega \\ Bu = g & \text{on } \Gamma_T := (0,T) \times \Gamma \\ u = u_0 & \text{in } \{0\} \times \Omega, \end{cases} \tag{3}$$

where $T > 0$, $f = f(t,x)$, $g = g(t,x)$, and $u_0 = u_0(x)$ are given data and $Bu = g$ denotes any of the admissible boundary conditions (Dirichlet, Neumann, or mixed types).

We indicate with $L^2(\Omega)$ the Hilbert space of measurable functions v which are square integrable. For any $v, w \in L^2(\Omega)$, we denote the associated inner product and norm as $(w,v) := \int_\Omega w(x)v(x)\mathrm{d}x$ and $\|w\|_{L^2(\Omega)} := \sqrt{(w,w)}$, respectively. Let V be a closed subspace of $H^1(\Omega)$ such that $H_0^1(\Omega) \subseteq V \subseteq H^1(\Omega)$. Denote by $(\cdot,\cdot)_{H^1(\Omega)}$ the inner product associated with $H^1(\Omega)$, i.e. $(w,v)_{H^1(\Omega)} := (w,v) + (\nabla w, \nabla v)$ for any $w, v \in H^1(\Omega)$ and define the norm $\|v\|_{H^1(\Omega)} := \sqrt{(v,v)_{H^1(\Omega)}}$ on V for any $v \in V$. In addition, we will need the Hilbert spaces $H^k(\Omega) := W^{k,2}(\Omega)$, for k a non-negative integer; accordingly, $(\cdot,\cdot)_{H^k(\Omega)}$, $\|\cdot\|_{H^k(\Omega)}$ and $|\cdot|_{H^k(\Omega)}$ will be used as their inner products, norms and seminorms, respectively (see e.g. [35]). We point out that each of the boundary conditions yields a specific choice of V. Now, let us consider boundary conditions of Dirichlet and mixed types. Thanks to the *Poincaré inequality*, when Dirichlet or mixed type boundary conditions are considered, there exists a constant $C_\Omega \in (0,1)$ such that

$$\|v\|_{L^2(\Omega)}^2 \leq C_\Omega \|v\|_{H^1(\Omega)}^2 \quad \forall v \in V. \tag{4}$$

We associate the operator L with a bilinear form

$$a(w,v) := \int_\Omega \left[\sum_{i,j=1}^{d} \tilde{a}_{ij} D_j w D_i v - \sum_{i=1}^{d} (b_i w D_i v - c_i v D_i w) + a_0 w v \right] \mathrm{d}x. \tag{5}$$

We first assume that a: $V \times V \to \mathbb{R}$ is a continuous and *weakly coercive* bilinear form, i.e. there exist constants $\alpha > 0$, $\beta > 0$ and $\lambda \geq 0$ such that

$$|a(u,v)| \leq \beta \|u\|_{H^1(\Omega)} \|v\|_{H^1(\Omega)} \quad \forall u, v \in V \tag{6}$$

and

$$a(v,v) + \lambda \|v\|_{L^2(\Omega)}^2 \geq \alpha \|v\|_{H^1(\Omega)}^2 \quad \forall v \in V, \tag{7}$$

respectively. The operator L of (2) is chosen in such a manner that the inequality (7) is assumed to be satisfied provided that the coefficients of L belong to $L^\infty(\Omega)$. Without loss of

generality, we can assume further that the bilinear form $a(\cdot,\cdot)$ satisfies (7) with $\lambda = 0$ by the change of variable $u_\lambda(t,x) = \mathrm{e}^{-\lambda t}u(t,x)$, for which the corresponding error estimates for the solution $u(t,x)$ in the following sections show an extra multiplicative factor $\mathrm{e}^{\lambda t}$ [35].

We denote with $L^2(0,T;V)$ the space of measurable functions $\phi : (0,T) \to V$ which are square integrable, i.e. $\int_0^T \|\phi(t)\|_V^2 \mathrm{d}t < \infty$, where $\phi(t) := \phi(t,\cdot)$ is considered as a function of the space variable only for t fixed; we also define the Hilbert space $W(0,T;V) := \{\phi \in L^2(0,T;V) \mid \phi_t \in L^2(0,T;V')\}$, where V' is the dual space of V. Finally, we denote the space of continuous functions $\phi : (0,T) \to L^2(\Omega)$ by $C^0([0,T];L^2(\Omega))$.

Given $f \in C^0([0,T];L^2(\Omega))$ and $u_0 \in L^2(\Omega)$, we consider, for our analysis, the following weak formulation of problem (3) with homogeneous Dirichlet boundary conditions for which $V = H_0^1(\Omega)$: find $u \in L^2(0,T;V) \cap C^0([0,T];L^2(\Omega))$ such that

$$\frac{\mathrm{d}}{\mathrm{d}t}(u(t),v) + a(u(t),v) = (f(t),v) \quad \forall v \in V \tag{8}$$

$$(u(0),\chi) = (u_0,\chi) \quad \forall \chi \in L^2(\Omega), \tag{9}$$

which admits a unique weak solution $u \in W(0,T;V)$. In addition, if $u_0 \in V$, we have $u \in C^0([0,T];V)$ and $u_t \in C^0([0,T];L^2(\Omega))$ (see e.g. [11]).

2.2 IGA space semi-discretization of PDE model

Let us introduce a spatial semi-discretization of (8) based on IGA [9]. We recall in the following some basic definitions and properties of IGA.

2.3 B-splines and NURBS of IGA

We start by recalling univariate B-splines and NURBS [33]. For any α $(1 \le \alpha \le d)$ and positive integer n_α, we define the *knot vector* $\Xi_\alpha := \{0 = \xi_{1,\alpha}, \xi_{2,\alpha}, \ldots, \xi_{n_\alpha+p_\alpha+1,\alpha} = 1\}$ consisting of nondecreasing *knots*, i.e. $\xi_{1,\alpha} \le \xi_{2,\alpha} \le \ldots \le \xi_{n_\alpha+p_\alpha+1,\alpha}$. Knots may be repeated with the number of repetitions called *multiplicity*. A knot vector is assumed to be *open* if both of the first and the last $p_\alpha + 1$ knots are repeated, where p_α is the polynomial degree. Denote by $B_{i,\alpha}$ $(i = 1,2,\ldots,n_\alpha)$ the *B-spline* basis functions, which can be generated by the recursive Cox-de Boor procedure [33]. Each B-spline basis function is everywhere pointwise C^∞-continuous except at knots $\xi_{i,\alpha}$, where it is $C^{p_\alpha-\kappa_{i,\alpha}}$-continuous if the multiplicity of the knot is $\kappa_{i,\alpha}$ with $1 \le \kappa_{i,\alpha} < p_\alpha + 1$. The B-spline basis functions are non-negative, locally supported in $(\xi_{i,\alpha}, \xi_{i+p_\alpha+1,\alpha})$ (the *knot span*), and constitute a partition of unity [22], i.e. $\sum_{i=1}^{n_\alpha} B_{i,\alpha} = 1$. We define the space of univariate B-splines $\mathscr{B}_\alpha \equiv \mathscr{B}(\Xi_\alpha; p_\alpha) := \mathrm{span}\{B_{i,\alpha}\}_{i=1,\ldots,n_\alpha}$. See e.g. Fig. 1 for a typical B-splines basis in the univariate case.

Multivariate tensor product B-splines are defined based on d knot vectors Ξ_α, $\alpha = 1,\ldots,d$. Let $\hat{\Omega} := (0,1)^d \subset \mathbb{R}^d$ be an open *parametric domain*. The knot vectors partition $\hat{\Omega}$ into "mesh" elements, which constitute a mesh $\mathscr{Q}_h \equiv \mathscr{Q}_h(\Xi_1,\ldots,\Xi_d) := \{Q = \otimes_{\alpha=1}^d (\xi_{i_\alpha,\alpha}, \xi_{i_\alpha+1,\alpha}) \mid p_\alpha + 1 \le i_\alpha \le n_\alpha - 1\}$. Let us denote $\hat{h}_Q := \mathrm{diam}(Q)$ for all $Q \in \mathscr{Q}_h$ and the global mesh size $\hat{h} := \max_{Q\in\mathscr{Q}_h}\{\hat{h}_Q\}$. For notational convenience, we denote a multi-index $\boldsymbol{i} := (i_1,\ldots,i_d)$ and a corresponding multi-index set $I := \{\boldsymbol{i} = (i_1,\ldots,i_d) \mid 1 \le i_\alpha \le n_\alpha \text{ for } 1 \le \alpha \le d\}$. Then, for each multi-index $\boldsymbol{i} \in I$, we define the tensor product B-spline

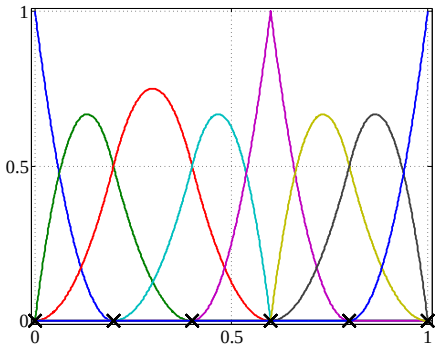

Fig. 1: Univariate quadratic B-spline basis functions with $n_1 = 8$ and $p_1 = 2$ generated from the knot vector $\Xi_1 = \{0,0,0,0.2,0.4,0.6,0.6,0.8,1,1,1\}$. The multiplicity of each interior knot is 1 except at $\xi_{i,1} = 0.6$; thus, the basis functions are C^1-continuous at the interior knots and C^0-continuous at the knots $\xi_{6,1} = \xi_{7,1} = 0.6$.

basis functions $B_{\boldsymbol{i}} : \hat{\Omega} \to \mathbb{R}$, $B_{\boldsymbol{i}} := B_{i_1,1} \otimes \ldots \otimes B_{i_d,d}$ and the corresponding tensor product B-splines space

$$\mathscr{B}_h \equiv \mathscr{B}_h(\Xi_1, \ldots, \Xi_d; p_1, \ldots, p_d) := \text{span}\{B_{\boldsymbol{i}}\}_{\boldsymbol{i} \in I}. \tag{10}$$

Notice that the functions in $\mathscr{B}_h$ are piecewise polynomials of degree p_α along each coordinate $\alpha = 1, \ldots, d$.

We associate the basis functions $B_{\boldsymbol{i}}$ with positive weights $\omega_{\boldsymbol{i}}$ and define a *weighting function* $\omega : \hat{\Omega} \to \mathbb{R}$, $\omega := \sum_{\boldsymbol{i} \in I} \omega_{\boldsymbol{i}} B_{\boldsymbol{i}}$. The NURBS basis functions in the parameter domain are defined by projection as

$$R_{\boldsymbol{i}} : \hat{\Omega} \to \mathbb{R}, \quad R_{\boldsymbol{i}} = \frac{\omega_{\boldsymbol{i}} B_{\boldsymbol{i}}}{\omega} \tag{11}$$

and the corresponding NURBS space over $\hat{\Omega}$ reads: $\mathscr{S}_h \equiv \mathscr{S}_h(\Xi_1, \ldots, \Xi_d; p_1, \ldots, p_d; \omega) := \text{span}\{R_{\boldsymbol{i}}\}_{\boldsymbol{i} \in I}$.

In order to perform a parameterization of the physical domain, we introduce the control points $\mathbf{C}_{\boldsymbol{i}} \in \mathbb{R}^d$ and define the *geometric mapping* $\mathbf{F} : \hat{\Omega} \to \Omega$ with $\mathbf{F} := \sum_{\boldsymbol{i} \in I} \mathbf{C}_{\boldsymbol{i}} R_{\boldsymbol{i}}$. Let us assume that $\mathbf{F}$ is invertible and possesses smooth inverse a.e. in $\hat{\Omega}$, e.g. in each element $Q \in \mathscr{Q}_h$. We define $\nabla \mathbf{F} : \hat{\Omega} \to \mathbb{R}^d$ and $J_{\mathbf{F}} : \hat{\Omega} \to \mathbb{R}$ to be the Jacobian matrix and determinant of map $\mathbf{F}$, respectively. By using $\mathbf{F}$, we define a *physical mesh* in the physical domain Ω, whose elements are obtained as the image of the elements in the parameteric domain, i.e. $\mathscr{K}_h := \{K = \mathbf{F}(Q) \mid Q \in \mathscr{Q}_h\}$. The corresponding mesh size in the physical domain is defined as $h := \max_{K \in \mathscr{K}_h} h_K$, where $h_K = \|\nabla \mathbf{F}\|_{L^\infty(Q)} h_Q$.

Furthermore, we define the space spanned by NURBS basis functions in Ω as the push-forward of the space $\mathscr{S}_h$, which reads:

$$\mathscr{V}_h \equiv \mathscr{V}_h(p_1, \ldots, p_\alpha) := \text{span}\{R_{\boldsymbol{i}} \circ \mathbf{F}^{-1}\}_{\boldsymbol{i} \in I} = \text{span}\{\mathscr{R}_{\boldsymbol{i}}\}_{\boldsymbol{i} \in I}, \tag{12}$$

where $\{\mathscr{R}_{\boldsymbol{i}}\}_{\boldsymbol{i} \in I}$ is the NURBS basis in the physical domain with $\mathscr{R}_{\boldsymbol{i}} := R_{\boldsymbol{i}} \circ \mathbf{F}^{-1}$ for all $\boldsymbol{i} \in I$. Let p be the minimum degree of B-splines and NURBS, defined as $p := \min_{1 \le \alpha \le d}\{p_\alpha\}$.

We recall the interpolation theory of NURBS proposed in [2] for obtaining interpolation error estimates of IGA. Given a function $\hat{v} \in L^2(\hat{\Omega})$, we define a *projective operator* over the B-splines space $\mathscr{B}_h$ as: $\Pi_{\mathscr{B}_h}$: $L^2(\hat{\Omega}) \to \mathscr{B}_h$, $\Pi_{\mathscr{B}_h} \hat{v} := \sum_{\boldsymbol{i} \in I} \rho_{\boldsymbol{i}}(\hat{v}) B_{\boldsymbol{i}}$, where the linear

functionals $\rho_i(\hat{v}) \in L^2(\hat{\Omega})'$ determine the dual basis for the set of B-splines, i.e. they are such that $\rho_j(B_i) = \delta_{i,j}$ for $i,j \in I$, with δ the Kronecker function. The corresponding projective operator over the NURBS space $\mathscr{S}_h$ in $\hat{\Omega}$ is defined by means of the definition of the NURBS basis functions in (11) through the weighting function ω:

$$\Pi_{\mathscr{S}_h} : L^2(\hat{\Omega}) \to \mathscr{S}_h, \quad \Pi_{\mathscr{S}_h}\hat{v} := \frac{\Pi_{\mathscr{S}_h}(\omega\hat{v})}{\omega}, \tag{13}$$

for all $\hat{v} \in L^2(\hat{\Omega})$. In this manner, the projective operator over the NURBS space $\mathscr{V}_h$, is defined as the push-forward of the operator $\Pi_{\mathscr{S}_h}$

$$\Pi_{\mathscr{V}_h} : L^2(\Omega) \to \mathscr{V}_h, \quad \Pi_{\mathscr{V}_h} v := (\Pi_{\mathscr{S}_h}(\hat{v}) \circ \mathbf{F}^{-1}. \tag{14}$$

Henceforth, let $\{\mathscr{Q}_h\}_h$ and $\{\mathscr{K}_h\}_h$ be regular and quasi-uniform families of meshes in the parametric $\hat{\Omega}$ and physical Ω domains, respectively. The quasi-uniform property implies that there exist positive constants C_1 and C_2 independent of h such that $C_1 h \leq h_K \leq C_2 h$ $\forall K \in \mathscr{K}_h$. Now, we recall the global interpolation error estimate of NURBS for IGA, which reads as follows ([42]).

Lemma 1 (Global interpolation error estimate) *Given the integers ℓ and σ, with $0 \leq \ell \leq p+1$, $\ell \leq \sigma$, $\ell \leq k_{\mathrm{m}}+1$, and $k_{\mathrm{m}} \geq 0$ the minimum regularity of basis functions (i.e. $C^{k_{\mathrm{m}}}$-continuous in Ω), we have*

$$|u - \Pi_{\mathscr{V}_h} u|_{H^\ell(\Omega)} \leq C(\Omega, k_{\mathrm{m}}) h^{\delta-\ell} \|u\|_{H^\sigma(\Omega)} \ \ \forall u \in H^\sigma(\Omega), \tag{15}$$

where $\delta = \min\{\sigma, p+1\}$ and the positive constant $C(\Omega, k_{\mathrm{m}})$ only depends on k_{m} and the shape of Ω, but not on its size.

In addition, we have the following IGA *global inverse inequalities*:

Lemma 2 (Global inverse inequality) *Let k and l be two integers such that $0 \leq k \leq l$, then we have*

$$\|v_h\|_{H^l(\Omega)} \leq C_{\mathscr{I}}\, h^{k-l} |v_h|_{H^k(\Omega)} \ \ \forall v_h \in \mathscr{V}_h, \tag{16}$$

with $C_{\mathscr{I}} = C_{\mathscr{I}}(\Omega, \|\nabla \boldsymbol{F}\|_{L^\infty(\hat{\Omega})}, C_1, k_{\mathrm{m}})$ for $k_{\mathrm{m}} \geq 0$.

Proof By using the *local inverse inequalities* (cf. Theorem 4.2 in [2]), there exists a positive constant $C_{\mathrm{s},k_{\mathrm{m}}}$ depending on the shape of Ω and k_{m} such that

$$\|v_h\|_{H^l(K)} \leq C_{\mathrm{s},k_{\mathrm{m}}} h_K^{k-l} \sum_{i=0}^{k} \|\nabla \mathbf{F}\|^{i-k}_{L^\infty(\mathbf{F}^{-1}(K))} |v|_{H^i(K)} \ \ \forall K \in \mathscr{K}_h, \ \forall v_h \in \mathscr{V}_h. \tag{17}$$

Then, for any $v_h \in \mathscr{V}_h$ we obtain from (17):

$$\begin{aligned} \|v_h\|^2_{H^l(\Omega)} &= \sum_{K \in \mathscr{K}_h} \|v_h\|^2_{H^l(K)} \\ &\leq \sum_{K \in \mathscr{K}_h} C^2_{\mathrm{s},k_{\mathrm{m}}} h_K^{2(k-l)} \left(\sum_{i=0}^{k} \|\nabla \mathbf{F}\|^{i-k}_{L^\infty(\mathbf{F}^{-1}(K))} |v_h|_{H^i(K)} \right)^2 \\ &\leq C^2_{\mathrm{s},k_{\mathrm{m}}} (C_1 h)^{2(k-l)} \sum_{K \in \mathscr{K}_h} \left(\sum_{i=0}^{k} \|\nabla \mathbf{F}\|^{2(i-k)}_{L^\infty(\mathbf{F}^{-1}(K))} \sum_{i=0}^{k} |v_h|^2_{H^i(K)} \right), \end{aligned} \tag{18}$$

where the quasi-uniform property of meshes and Cauchy-Schwarz inequality are used in the last inequality. Finally, (18) implies that

$$\begin{aligned}\|v_h\|^2_{H^l(\Omega)} &\leq C^2_{\mathscr{J}}(\Omega, \|\nabla \mathbf{F}\|_{L^\infty(\hat{\Omega})}, C_1, k_{\mathrm{m}})\, h^{2(k-l)} \sum_{K\in\mathscr{K}_h} \sum_{i=0}^{k} |v_h|^2_{H^i(K)} \\ &= C^2_{\mathscr{J}}\, h^{2(k-l)} |v_h|^2_{H^k(\Omega)}. \qquad \square\end{aligned}$$

Remark 1 In several circumstances, IGA possesses a significant geometrical advantage with respect to the FEM since most of the computational domains of practical interest can be exactly represented by NURBS. The important case of conic sections is included in NURBS-based IGA. In this case, the geometrical representation of Ω allowed by FEM introduce numerical errors, which may lead to a loss of accuracy of the method, as it may be often seen in terms of reduced convergence orders of the errors under h-refinement [2,9,10,22]. Moreover, NURBS-based IGA possesses the advantage of yielding highly accurate approximations when using C^{p-1}-continuous basis functions with respect to C^0-continuous basis functions for smooth solutions of PDEs [4,10,15,23,42].

2.4 Spatial semi-discretization of IGA for parabolic problem

Let V_h be the finite-dimensional subspace of V such that $V_h = V \cap \mathscr{V}_h$. A general spatial semi-discrete Galerkin approximation of (8) reads: for any given $t \in (0,T]$, find $u^h(t) \in V_h$ such that

$$\begin{cases} \dfrac{\mathrm{d}}{\mathrm{d}t}(u_h(t), v_h) + a(u_h(t), v_h) = (f(t), v_h) \quad \forall v_h \in V_h \\ u_h(0) = u_{0,h}, \end{cases} \tag{19}$$

where $u_{0,h}$ is the L^2-projection of u_0 onto $\mathscr{V}_h$.

Let us first define an *elliptic "projection" operator* $\mathscr{P}^p_{1,h} : V \to V_h$ for each $v \in V$:

$$a(\mathscr{P}^p_{1,h} v, v_h) = a(v, v_h) \quad \forall v_h \in V_h, \tag{20}$$

from which we obtain the Galerkin orthogonality

$$a(v - \mathscr{P}^p_{1,h} v, v_h) = 0 \quad \forall v_h \in V_h. \tag{21}$$

We derive the following result.

Lemma 3 *Assume that (7) is satisfied with $\lambda = 0$ and that the solution φ_s of the adjoint problem*

$$find\ \varphi_s \in V :\ a(v, \varphi_s) = (s, v) \quad \forall v \in V \tag{22}$$

satisfies $\varphi_s \in H^2(\Omega)$ when $s \in L^2(\Omega)$. Then, there exists a positive constant $c = c(\Omega, \alpha, \beta, k_{\mathrm{m}})$ such that

$$\|v - \mathscr{P}^p_{1,h} v\|_{L^2(\Omega)} + h\|v - \mathscr{P}^p_{1,h} v\|_{H^1(\Omega)} \leq c\, h^{p+1} |v|_{H^{p+1}(\Omega)} \quad \forall v \in H^{p+1} \cap V. \tag{23}$$

Proof We proceed by estimating the two terms on the left-hand side of (23) separately. Firstly, we estimate the second term. From the coercivity property, Eq. (21), and continuity of $a(\cdot,\cdot)$, we obtain for any $v \in H^{p+1}(\Omega) \cap V$

$$\begin{aligned} \|v - \mathscr{P}^p_{1,h} v\|^2_{H^1(\Omega)} &\leq \frac{1}{\alpha} a(v - \mathscr{P}^p_{1,h} v, v - \mathscr{P}^p_{1,h} v) \\ &= \frac{1}{\alpha} a(v - \mathscr{P}^p_{1,h} v, v - w_h) \\ &\leq \frac{\beta}{\alpha} \|v - \mathscr{P}^p_{1,h} v\|_{H^1(\Omega)} \|v - w_h\|_{H^1(\Omega)} \quad \forall w_h \in V_h, \end{aligned} \tag{24}$$

which implies that

$$\|v - \mathscr{P}^p_{1,h} v\|_{H^1(\Omega)} \leq \frac{\beta}{\alpha} \inf_{w_h \in V_h} \|v - w_h\|_{H^1(\Omega)} \leq \frac{\beta}{\alpha} \|v - \Pi_{\mathscr{V}_h} v\|_{H^1(\Omega)}. \tag{25}$$

By using Lemma 1 with $\sigma = p+1$, we have for (25) that there exists a constant $c(\Omega, \alpha, \beta, k_{\mathrm{m}}) > 0$ such that

$$\|v - \mathscr{P}^p_{1,h} v\|_{H^1(\Omega)} \leq c(\Omega, \alpha, \beta, k_{\mathrm{m}}) h^p |v|_{H^{p+1}(\Omega)} \quad \forall v \in H^{p+1}(\Omega), \tag{26}$$

where $c(\Omega, \alpha, \beta, k_{\mathrm{m}}) = \alpha^{-1} \beta C(\Omega, k_{\mathrm{m}})$. To estimate $\|v - \mathscr{P}^p_{1,h} v\|_{L^2(\Omega)}$, we use the *Aubin-Nitsche duality argument*. By the assumption on the adjoint problem (22), we show that there exists a positive constant $C(\Omega, \alpha, \beta, k_{\mathrm{m}})$ suth that

$$\|v - \mathscr{P}^p_{1,h} v\|_{L^2(\Omega)} \leq C(\Omega, \alpha, \beta, k_{\mathrm{m}}) h^{p+1} |v|_{H^{p+1}(\Omega)} \quad \forall v \in H^{p+1}(\Omega). \tag{27}$$

In fact, by definition of L^2-norm and by replacing v with $v - \mathscr{P}^p_{1,h} v$ in (22), we have

$$\|v - \mathscr{P}^p_{1,h} v\|_{L^2(\Omega)} = \sup_{0 \neq s \in L^2(\Omega)} \frac{(s, v - \mathscr{P}^p_{1,h} v)}{\|s\|_{L^2(\Omega)}} = \sup_{0 \neq s \in L^2(\Omega)} \frac{a(v - \mathscr{P}^p_{1,h} v, \varphi_s)}{\|s\|_{L^2(\Omega)}}. \tag{28}$$

Then, it follows from Eq. (21) that for any $v_h \in V_h$,

$$\begin{aligned} \|v - \mathscr{P}^p_{1,h} v\|_{L^2(\Omega)} &= \sup_{0 \neq s \in L^2(\Omega)} \frac{a(v - \mathscr{P}^p_{1,h} v, \varphi_s - v_h)}{\|s\|_{L^2(\Omega)}} \\ &\leq \beta \|v - \mathscr{P}^p_{1,h} v\|_{H^1(\Omega)} \sup_{0 \neq s \in L^2(\Omega)} \frac{\|\varphi_s - v_h\|_{H^1(\Omega)}}{\|s\|_{L^2(\Omega)}}. \end{aligned} \tag{29}$$

By replacing v_h with $\Pi_{\mathscr{V}_h} \phi_s$, we have from Eq. (15)

$$\|\varphi_s - \Pi_{\mathscr{V}_h} \varphi_s\|_{H^1(\Omega)} \leq C(\Omega, k_{\mathrm{m}}) h \|\phi_s\|_{H^2(\Omega)}, \tag{30}$$

which implies that from Eq. (29)

$$\|v - \mathscr{P}^p_{1,h} v\|_{L^2(\Omega)} \leq C(\Omega, \beta, k_{\mathrm{m}}) h \|v - \mathscr{P}^p_{1,h} v\|_{H^1(\Omega)} \tag{31}$$

after using the regularity assumption for the adjoint problem. A combination of (31) and (26) yields (27) and therefore the result (23). □

Then, we have the error estimate between exact solution $u(t)$ and spatial semi-discrete approximation $u_h(t)$.

Theorem 1 *Let the hypotheses of Lemma 3 hold and assume that $f \in C^0([0,T];L^2(\Omega))$, $u_0 \in H^{p+1}(\Omega)$, $p \geq 1$, and the solution u of (8) is such that $u \in C^0([0,T];H^{p+1}(\Omega))$ and $\partial u/\partial t \in L^1(0,T;H^{p+1}(\Omega))$. Then, by using piecewise polynomials of degree less than or equal to p in definition of NURBS space $\mathcal{V}_h$, the solutions u and u_h to (8) and (19) satisfy respectively*

$$\begin{aligned} &\|u(t)-u_h(t)\|_{L^2(\Omega)} + h\|u(t)-u_h(t)\|_{H^1(\Omega)} \\ &\qquad \leq Ch^{p+1}\left(\|u_0\|_{H^{p+1}(\Omega)} + \int_0^t \left\|\frac{\partial u}{\partial t}(\tau)\right\|_{H^{p+1}(\Omega)} \mathrm{d}\tau\right) \end{aligned} \tag{32}$$

for each $t \in [0,T]$, where $C = C(\Omega,\alpha,\beta,k_{\mathrm{m}})$ is a positive constant independent of h.

Proof For any fixed $t \in (0,T]$, let us write

$$\begin{aligned} e_h(t) := u(t)-u_h(t) &= (u(t)-\mathscr{P}^p_{1,h}u(t)) + (\mathscr{P}^p_{1,h}u(t)-u_h(t)), \\ &\equiv w_1(t)+w_2(t) \end{aligned} \tag{33}$$

where $w_1(t) := u(t)-\mathscr{P}^p_{1,h}u(t)$ and $w_2(t) := \mathscr{P}^p_{1,h}u(t)-u_h(t)$. We estimate $w_1(t)$ from inequality (23) of Lemma 3 as

$$\begin{aligned} \|w_1(t)\|_{L^2(\Omega)} + h\|w_1(t)\|_{H^1(\Omega)} &\leq ch^{p+1}\|u(t)\|_{H^{p+1}(\Omega)} \\ &\leq ch^{p+1}\left(\|u_0\|_{H^{p+1}(\Omega)} + \int_0^t \left\|\frac{\partial u}{\partial t}(\tau)\right\|_{H^{p+1}(\Omega)} \mathrm{d}\tau\right). \end{aligned} \tag{34}$$

To estimate $\|w_2(t)\|_{L^2(\Omega)}$, we have from Eqs. (8), (19), and (21), for any $v_h \in V_h$

$$\begin{aligned} \left(\frac{\partial w_2}{\partial t}(t), v_h\right) + a(w_2(t),v_h) &= \left(\frac{\partial}{\partial t}[\mathscr{P}^p_{1,h}u(t)], v_h\right) + a(\mathscr{P}^p_{1,h}u(t), v_h) \\ &\quad - \left(\frac{\partial u_h}{\partial t}(t), v_h\right) - a(u_h(t),v_h) \\ &= \left(\frac{\partial}{\partial t}[\mathscr{P}^p_{1,h}u(t)], v_h\right) - \left(\frac{\partial u}{\partial t}, v_h\right) = -\left(\frac{\partial w_1}{\partial t}(t), v_h\right). \end{aligned}$$

By replacing v_h with $w_2(t)$ for fixed $t \in (0,T]$, it follows that

$$\frac{1}{2}\frac{\mathrm{d}}{\mathrm{d}t}\|w_2(t)\|^2_{L^2(\Omega)} + a(w_2(t),w_2(t)) = -\left(\frac{\partial w_1}{\partial t}(t), w_2(t)\right). \tag{35}$$

Then, we have by (7) and the Cauchy-Schwarz inequality

$$\begin{aligned} \frac{1}{2}\frac{\mathrm{d}}{\mathrm{d}t}\|w_2(t)\|^2_{L^2(\Omega)} + \alpha\|w_2(t)\|^2_{H^1(\Omega)} &\leq -\left(\frac{\partial w_1}{\partial t}(t), w_2(t)\right) \\ &\leq \left\|\frac{\partial w_1}{\partial t}(t)\right\|_{L^2(\Omega)} \|w_2(t)\|_{L^2(\Omega)}. \end{aligned} \tag{36}$$

Therefore, by neglecting $\alpha\|w_2(t)\|^2_{H^1(\Omega)}$ on the left-hand side, cancelling $\|w_2(t)\|_{L^2(\Omega)}$ on both the sides and integrating over $[0,t]$ gives

$$\begin{aligned}\|w_2(t)\|_{L^2(\Omega)} &\le \|w_2(0)\|_{L^2(\Omega)} + \int_0^t \left\| \frac{\partial w_1}{\partial t}(\tau) \right\|_{L^2(\Omega)} \mathrm{d}\tau \\ &\le \|\mathscr{P}^p_{1,h} u_0 - u_0\|_{L^2(\Omega)} + \|u_0 - u_{0,h}\|_{L^2(\Omega)} + \int_0^t \left\| \frac{\partial w_1}{\partial t}(\tau) \right\|_{L^2(\Omega)} \mathrm{d}\tau \qquad (37) \\ &\le (c + C(\Omega, k_{\mathrm{m}}))h^{p+1}\|u_0\|_{H^{p+1}(\Omega)} + ch^{p+1}\int_0^t \left\| \frac{\partial u}{\partial t}(\tau) \right\|_{H^{p+1}(\Omega)} \mathrm{d}\tau,\end{aligned}$$

where we have used the inequalities (15) and (23) and the fact that the time derivative commutes with $\mathscr{P}^p_{1,h}$. Then, we use the triangle inequality $\|e_h\|_{L^2(\Omega)} \le \|w_1\|_{L^2(\Omega)} + \|w_2\|_{L^2(\Omega)}$, (37), and (34) to obtain the error estimate of $\|u(t) - u_h(t)\|_{L^2(\Omega)}$ in (32).

Now, we estimate $\|e_h(t)\|_{H^1(\Omega)}$ based on the bounds of $\|e_h(t)\|_{L^2(\Omega)}$ we have just obtained. In fact, we have, for any $v_h \in V_h$

$$\begin{aligned}\|e_h(t)\|_{H^1(\Omega)} &\le \|u(t) - v_h\|_{H^1(\Omega)} + \|v_h - u_h(t)\|_{H^1(\Omega)} \\ &\le \|u(t) - v_h\|_{H^1(\Omega)} + C_{\mathscr{I}} h^{-1}\|v_h - u_h(t)\|_{L^2(\Omega)} \qquad \text{(Lemma 2)} \\ &\le C_{\mathscr{I}} h^{-1}(\|v_h - u(t)\|_{L^2(\Omega)} + h\|u(t) - v_h\|_{H^1(\Omega)}) + C_{\mathscr{I}} h^{-1}\|e_h(t)\|_{L^2(\Omega)} \\ &\le C_{\mathscr{I}} h^{-1} C(\Omega, k_{\mathrm{m}}) h^{p+1}\|u(t)\|_{H^{p+1}(\Omega)} \\ &\quad + C_{\mathscr{I}} h^{-1} C h^{p+1}\left(\|u_0\|_{H^{p+1}(\Omega)} + \int_0^t \left\| \frac{\partial u}{\partial t}(\tau) \right\|_{H^{p+1}(\Omega)} \mathrm{d}\tau \right) \\ &\le C h^p \left(\|u_0\|_{H^{p+1}(\Omega)} + \int_0^t \left\| \frac{\partial u}{\partial t}(\tau) \right\|_{H^{p+1}(\Omega)} \mathrm{d}\tau \right)\end{aligned}$$

with $C = C(\Omega, \alpha, \beta, k_{\mathrm{m}})$, where we have used Lemma 1 and the error estimator (32) for $\|e_h(t)\|_{L^2(\Omega)}$ in the last second inequality. □

The IGA spatial semi-discretized problem (19) is a system of ordinary differential equations. Let us denote by N_x the number of degrees of freedom of the finite dimensional space V_h. Renumber each $\boldsymbol{i} \in I$ from 1 to N_x. By writting $u_h(t) = \sum_{j=1}^{N_x} d_j(t)\mathscr{R}_j$ and $u_{0,h} = \sum_{j=1}^{N_x} d_{0,j}\mathscr{R}_j$ and taking $v_h = \mathscr{R}_i$ $(i = 1, \ldots, N_x)$, problem (19) then turns to

$$\begin{cases} M\dot{d}(t) + Ad(t) = f(t),\ t \in (0,T] \\ d(0) = d_0, \end{cases} \qquad (38)$$

where

$$\begin{aligned} &A = [a_{ij}] \in \mathbb{R}^{N_x \times N_x},\ a_{ij} = a(R_j, R_i),\ \ M = [m_{ij}] \in \mathbb{R}^{N_x \times N_x},\ m_{ij} = \int_\Omega R_j R_i \mathrm{d}x, \\ &d(t) = (d_1(t), \ldots, d_{N_x}(t))^{\mathrm{T}} \in \mathbb{R}^{N_x},\ d_0 = (d_{0,1}, \ldots, d_{0,N_x})^{\mathrm{T}} \in \mathbb{R}^{N_x}, \\ &f(t) = (f_1(t), \ldots, f_{N_x}(t))^{\mathrm{T}} \in \mathbb{R}^{N_x}, f_i(t) = \int_\Omega f(t) R_i \mathrm{d}x, \end{aligned}$$

with $1 \le i, j \le N_x$.

We now introduce a weighted inner product in $\mathbb{R}^{N_x}$ for the IGA control variables to replace the inner products in the finite-dimensional (N_x-dimensional) space V_h. The induced

norms are also changed correspondingly. Let us consider two arbitrary vectors $\boldsymbol{c},\boldsymbol{d}\in\mathbb{R}^{N_x}$, with $\boldsymbol{c}=(c_i)_{1\le i\le N_x}$ and $\boldsymbol{d}=(d_i)_{1\le i\le N_x}$, then we define the weighted inner product $\langle\cdot,\cdot\rangle_{\mathrm{W}}$ in $\mathbb{R}^{N_x}$ as

$$\langle \boldsymbol{c},\boldsymbol{d}\rangle_W := \boldsymbol{c}^{\mathrm{T}} W \boldsymbol{d} = \sum_{i=1}^{N_x}\sum_{j=1}^{N_x} c_i W_{ij} d_j, \tag{39}$$

where $W=[w_{ij}]_{1\le i,j\le N_x}\in\mathbb{R}^{N_x\times N_x}$ denotes a symmetric positive definite weight matrix. We then denote the induced norm $|\cdot|_W := \langle\cdot,\cdot\rangle^{1/2}$. Since $u_h(x)=\sum_{i=1}^{N_x} d_i\mathscr{R}_i(x)$ and $v_h(x)=\sum_{i=1}^{N_x} c_i\mathscr{R}_i(x)$ are elements of the finite-dimensional subspace $V_h\subset\mathbb{R}^{N_x}$ of V, we have $(u_h,v_h)=\langle\boldsymbol{d},\boldsymbol{c}\rangle_W$ and $\|u_h\|_{L^2(\Omega)}=|\boldsymbol{d}|_W$ with $W=M$. Analogously, we obtain $(u_h,v_h)_V=\langle\boldsymbol{d},\boldsymbol{c}\rangle_W$ and $\|u_h\|_{H^1(\Omega)}=|\boldsymbol{d}|_W$ with $W=M+A$.

2.5 Full space-time discretization of PDE model

We now apply the θ-scheme with $\theta\in[0,1]$ for the time discretization of problem (19) (see e.g. [35]). For $N_t\in\mathbb{N}$, we introduce a time step $\Delta t=T/N_t$ and uniform discrete time instances $t_n=n\Delta t$ for $n=0,1,\dots,N_t$. Three widely used special θ-schemes are: *forward Euler* ($\theta=0$, explicit, error of order $\mathscr{O}(\Delta t)$); *backward Euler* ($\theta=1$, implicit, $\mathscr{O}(\Delta t)$); *Crank-Nicolson* ($\theta=1/2$, implicit, $\mathscr{O}(\Delta t^2)$). Let us denote $u^n=u(t_n)$ and $f^n=f(t^n)$, $n=0,\dots,N_t$. For notational simplification, the superscript "$n+\theta$"of an arbitrary quantity, e.g. ζ, means that

$$\zeta^{n+\theta} := \theta\zeta^{n+1}+(1-\theta)\zeta^n.$$

Instead, when $\bar\partial$ is associated with an arbitrary quantity ζ^n, we mean forward differences

$$\bar\partial\zeta^n := \frac{1}{\Delta t}(\zeta^{n+1}-\zeta^n).$$

Then, we have the following IGA-θ full space-time discretization scheme for problem (38): find $u_h^n\in V_h$ such that

$$\begin{cases} \left(\bar\partial u_h^n, v_h\right)+a(u_h^{n+\theta},v_h)=(f^{n+\theta},v_h) \quad \forall v_h\in V_h,\ n=0,\dots,N_t-1\\ u_h^0=u_{0,h}. \end{cases} \tag{40}$$

Its algebraic counterpart reads: find $\{\boldsymbol{d}_h^n\}_{n=1}^{N_t}\subset V_h$ such that

$$\begin{cases} M\bar\partial\boldsymbol{d}_h^n+A\boldsymbol{d}_h^{n+\theta}=\boldsymbol{f}^{n+\theta}, \quad n=0,\dots,N_t-1,\\ \boldsymbol{d}_h^0=\boldsymbol{d}_{0,h}, \end{cases} \tag{41}$$

where $\boldsymbol{d}_h^n=(d_{h,1}^n,\dots,d_{h,N_x}^n)^{\mathrm{T}}$ for $n=0,1,\dots,N_t$.

The θ-scheme is unconditionally stable for $\theta\in[1/2,1]$, whereas a restriction between the time step and mesh size should be satisfied when $\theta\in[0,1/2)$. Moreover, we have the following two results on L^2-stability and convergence, respectively.

Lemma 4 (IGA-θ Stability) *Assume the map $t\to\|f(t)\|_{L^2(\Omega)}$ is bounded in $[0,T]$. Let $\theta\in[0,1]$. Moreover, when $\theta\in[0,1/2)$ let the time step Δt satisfy the condition*

$$\Delta t(1+C_{\mathscr{I}}h^{-2})\le\frac{2\alpha}{(1-2\theta)\beta^2}, \tag{42}$$

where α, β, and $C_{\mathscr{I}}$ are defined in (6), (7), and (16), respectively. Then, the solution u_h^n of fully discrete problem (40) satisfies

$$\|u_h^n\|_{L^2(\Omega)} \leq \underline{C}\left(\|u_{0,h}\|_{L^2(\Omega)} + \sup_{t\in[0,T]}\|f(t)\|_{L^2(\Omega)}\right), \quad n=0,1,\ldots,N_t, \tag{43}$$

where the constant $\underline{C}$ is a non-decreasing function of α^{-1}, β and T, and is independent of N_t, Δt, and h.

Proof The result holds by following a similar proof as Theorem 11.3.1 [35], which corresponds to the FEM-θ discrete scheme. □

Lemma 5 (Convergence) *Let the assumptions of Lemma 4 hold. Assume further that $\partial u_h(0)/\partial t \in L^2(\Omega)$, $f \in L^2(\Omega_T)$ with $\partial f/\partial t \in L^2(\Omega)$. Then, the functions $u_h(t)$ and u_h^n defined in (19) and (40), respectively, satisfy*

$$\|u_h(t_n) - u_h^n\|_{L^2(\Omega)} \leq C_\theta \Delta t \left(\left\|\frac{\partial u_h}{\partial t}(0)\right\|_{L^2(\Omega)} + \left\|\frac{\partial f}{\partial t}\right\|_{L^2(0,T;L^2(\Omega))}\right) \tag{44}$$

for $n=0,1,\ldots,N_t$. When $\theta = 1/2$, under the additional assumptions $\partial^2 f/\partial t^2 \in L^2(\Omega_T)$ and $\partial^2 u_h/\partial t^2 \in L^2(\Omega)$, we have

$$\|u_h(t_n) - u_h^n\|_{L^2(\Omega)} \leq C(\Delta t)^2 \left(\left\|\frac{\partial^2 u_h}{\partial t^2}(0)\right\|_{L^2(\Omega)} + \left\|\frac{\partial^2 f}{\partial t^2}\right\|_{L^2(0,T;L^2(\Omega))}\right) \tag{45}$$

for $n=0,1,\ldots,N_t$. The positive constants C_θ and C are non-decreasing functions of α^{-1}, β and T, and depend also on k_{m}, while are independent of Δt and h.

Proof The proof follows similarly to the proofs of Theorems 11.3.1 and 11.3.2 in [35] by considering separately the cases $0 \leq \theta < 1/2$ and $1/2 \leq \theta \leq 1$. The inverse inequality for FEM discretization is replaced by that for the IGA discretization (i.e. Lemma 2). □

We provide the following *a priori* error estimates for the fully-discrete approximation.

Theorem 2 *Let the assumptions in Theorem 1, Lemmas 4 and 5 be satisfied. Then, there exist positive constants $\tilde{C}_\theta$ and $\tilde{C}$ depending on α, β, k_{m} and T, and independent of Δt and h such that*

$$\begin{aligned}\|u(t_n) - u_h^n\|_{L^2(\Omega)} \leq & \tilde{C}_\theta \left[h^{p+1}\left(|u_0|_{H^{p+1}(\Omega)} + \left\|\frac{\partial u}{\partial t}\right\|_{L^1(0,T;H^{p+1}(\Omega))}\right)\right. \\ & \left. + \Delta t\left(\left\|\frac{\partial u_h}{\partial t}(0)\right\|_{L^2(\Omega)} + \left\|\frac{\partial f}{\partial t}\right\|_{L^2(0,T;L^2(\Omega))}\right)\right],\end{aligned} \tag{46}$$

and in the particular case $\theta = 1/2$,

$$\begin{aligned}\|u(t_n) - u_h^n\|_{L^2(\Omega)} \leq & \tilde{C}\left[h^{p+1}\left(|u_0|_{H^{p+1}(\Omega)} + \left\|\frac{\partial u}{\partial t}\right\|_{L^1(0,T;H^{p+1}(\Omega))}\right)\right. \\ & \left. + (\Delta t)^2\left(\left\|\frac{\partial^2 u_h}{\partial t^2}(0)\right\|_{L^2(\Omega)} + \left\|\frac{\partial^2 f}{\partial t^2}\right\|_{L^2(0,T;L^2(\Omega))}\right)\right].\end{aligned} \tag{47}$$

Proof The results follow by combining Theorem 1 and Lemma 5. □

3 POD for parameterized PDEs

Model order reduction of parameterized PDEs aims at reducing the dimension of solution manifolds corresponding to sets of time, physical and geometric parameters for steady and/or unsteady problems. In this paper, we limit to the case of a single parameter which is the time variable. POD-Galerkin methods for numerical solutions of PDEs usually demand to firstly obtain or train a POD basis in which the number of basis functions is expected to be much smaller than that in the full order Galerkin approximation, e.g. FEM. There are two types of POD basis generation approaches [44]: the continuous POD (C-POD) and discrete POD (D-POD), the latter, also known as the method of snapshots, is the approach we consider in this paper.

3.1 D-POD

A continuous and accurate set of snapshots $\{y(t)\,|\,t\in[0,T]\}$ is usually not available in practice and it needs to be realized by available discrete approximate snapshots (e.g. in our case (8)):

$$\{y_j\,|\,y_j=u_h^{j-1}, j=1,\ldots,N_t+1\}\subset X_h. \tag{48}$$

Here, h is the mesh parameter related to a specific spatial discretization method, $u_h^j\simeq u(t_j)$ with $t_j=j\Delta t$ and X_h is a finite-dimensional subspace of X. We compute numerical approximations of $y(t)$ by a full discretization method consisting of spatial IGA approximation and θ-method, dicussed in detail in Section 2. Denote $\mathscr{V}_{\ell_d}:=\operatorname{span}\{y_j\,|\,y_j=u_h^{j-1}, j=1,\ldots,N_t+1\}$ and $\ell_d:=\dim\mathscr{V}_d\le N_t+1<\infty$ (in some instances $\ell_d<N_t+1$, since snapshots may be linearly dependent). For $r\in\{1,\ldots,\ell_d\}$, the D-POD requires to solve a *finite-dimensional* optimization problem

$$\begin{aligned}&\min_{\{\varphi_k\}_{k=1}^r\subset X_h}\sum_{j=1}^{N_s}\alpha_j\left\|y_j-\sum_{k=1}^{r}(y_j,\varphi_k)_X\,\varphi_k\right\|_X^2\\&\text{subject to }(\varphi_i,\varphi_j)_X=\delta_{ij}\text{ for }1\le i,j\le r\end{aligned} \tag{49}$$

to obtain an optimal orthonormal basis $\{\varphi_i\}_{i=1}^r$, where the number of snapshots $N_s=N_t+1$ at this stage and $\{\alpha_j\}_{j=1}^{N_t+1}$ denote nonnegative weights satisfying $\sum_{j=1}^{N_t+1}\alpha_j=T$. Specifically, we choose trapezoidal weights as in [44], i.e.

$$\alpha_1=\alpha_{N_t+1}=\frac{\Delta t}{2}\quad\text{and}\quad\alpha_i=\Delta t,\ \text{ for }\ i=2,\ldots,N_t, \tag{50}$$

which ensures that (49) is an approximation of a time integral when Δt is small.

3.2 Time derivatives (TD) and time difference quotients (TDQ)

Recently, TD/TDQ were suggested to be included in the set of snapshots in analysis of the C/D-POD truncation errors [27,20,41]. For D-POD with TDQ included, the set of snapshots $\{y_j\}_{j=1}^{N_s}$ with $N_s=2N_t+1$ consists of numerical solutions

$$y_j=u_h^{j-1},\ \ j=1,\ldots,N_t+1$$

plus their TDQ counterpart

$$y_j = \bar{\partial} u_h^{j-N_t-2}, \quad j = N_t+2, \ldots, N_s. \tag{51}$$

It is well-known that these TDQ can be regarded as second-order central difference approximations at $t_{i-1/2} := (i-1/2)\Delta t$ for $i = 1, \ldots, N_t$. Then, the additional weights $\{\alpha_j\}_{j=N_t+2}^{N_s}$ in problem (49) arising with TDQ, are $\alpha_j = \Delta t$ for $j = N_t+2, \ldots, N_s$. We set $\mathscr{V}_{\ell_d} \equiv \text{span}\{\bar{y}_j\}_{j=1}^{\ell_d}$, where $\{\bar{y}_j\}_{j=1}^{\ell_d}$ denote the linearly independent basis obtained from $\text{span}\{y_j\}_{j=1}^{N_s}$ and refer to $\mathscr{V}_{\ell_d}$ as the set consisting of the snapshots $\{y_j\}_{j=1}^{N_s}$. Notice that the inclusion of TDQ approximately doubles the cardinality of snapshot set but does not change the dimension of the space, which is spanned by snapshots without TDQ. Kunisch and Volkwein [27] showed that it is necessary to include TDQ for convergence analysis of POD-Galerkin schemes (see the *Remark 1* in [27]). Iliescu and Wang [25] numerically showed that including TDQ in the construction of POD basis can lead to a higher convergence rate with respect to the POD rank than that in the standard case without TDQ.

We introduce the so-called *correlation matrix*

$$K = [k_{ij}] \in \mathbb{R}^{N_s \times N_s} \ \text{ with } \ k_{ij} = \frac{1}{N_s}(y_j, y_i)_X, \tag{52}$$

where K is symmetric positive semi-definite and has rank ℓ_d since $\dim \mathscr{V}_{\ell_d} = \ell_d$. Let $\lambda_1 \geq \ldots \geq \lambda_{\ell_d} > 0$ denote the eigenvalues of K and $\lambda_{\ell_d+1} = \ldots = \lambda_{N_s} = 0$ the null ones, then, $v_1, \ldots, v_{\ell_d} \in \mathbb{R}^{N_s}$ are the associated eigenvectors. Then, a POD basis of rank r with $1 \leq r \leq \ell_d$ (i.e. the solution of problem (49) with/without TDQ) is given by

$$\psi_k = \frac{1}{\sqrt{N_s \lambda_k}} \sum_{j=1}^{N_s} (v_k)_j y_j, \quad k = 1, \ldots, r. \tag{53}$$

Moreover, we have the following error formula for the general D-POD from snapshots with or without TDQ:

$$\frac{1}{N_s} \sum_{j=1}^{N_s} \left\| y_j - \sum_{k=1}^{r} (y_j, \psi_k)_X \psi_k \right\|_X^2 = \sum_{k=r+1}^{\ell_d} \lambda_k. \tag{54}$$

Specifically, for the TDQ-based D-POD, we have different versions of Eq. (54) for different choices of X. Let $\hat{\lambda}_k$ and $\tilde{\lambda}_k$, $k = 1, \ldots, \ell_d$ denote the eigenvalues of the correlation matrix K with $X = L^2(\Omega)$ and $X = H^1(\Omega)$, respectively. For $X = L^2(\Omega)$, we denote by $\{\hat{\psi}_k\}_{k=1}^{\ell_d}$ the POD basis and (54) implies that

$$\begin{aligned} &\frac{1}{2N_t+1} \sum_{n=0}^{N_t} \left\| u_h^n - \sum_{k=1}^{r} (u_h^n, \hat{\psi}_k) \hat{\psi}_k \right\|_{L^2(\Omega)}^2 \\ &\quad + \frac{1}{2N_t+1} \sum_{n=0}^{N_t-1} \left\| \bar{\partial} u_h^n - \sum_{k=1}^{r} (\bar{\partial} u_h^n, \hat{\psi}_k) \hat{\psi}_k \right\|_{L^2(\Omega)}^2 = \sum_{k=r+1}^{\ell_d} \hat{\lambda}_k. \end{aligned} \tag{55}$$

For $X = H^1(\Omega)$, we denote by $\{\tilde{\psi}_k\}_{k=1}^{\ell_d}$ the POD basis and (54) leads to

$$\begin{aligned} &\frac{1}{2N_t+1} \sum_{n=0}^{N_t} \left\| u_h^n - \sum_{k=1}^{r} (u_h^n, \tilde{\psi}_k)_{H^1(\Omega)} \tilde{\psi}_k \right\|_{H^1(\Omega)}^2 \\ &\quad + \frac{1}{2N_t+1} \sum_{n=0}^{N_t-1} \left\| \bar{\partial} u_h^n - \sum_{k=1}^{r} (\bar{\partial} u_h^n, \tilde{\psi}_k)_{H^1(\Omega)} \tilde{\psi}_k \right\|_{H^1(\Omega)}^2 = \sum_{k=r+1}^{\ell_d} \tilde{\lambda}_k. \end{aligned} \tag{56}$$

It is obvious that the POD basis and eigenvalues above for both cases $X = L^2(\Omega)$ and $X = H^1(\Omega)$ depend on the discretization parameters h and Δt. In the following, if we do not distinguish between the two bases in $L^2(\Omega)$ and $H^1(\Omega)$, we will generally write $\{\psi_i\}_{i=1}^r$ and denote by $V_r := \text{span}\{\psi_1, \psi_2, \ldots, \psi_r\}$ the *POD space of dimension r* with $V_r \subset \mathscr{V}_{\ell_d}$ for $r < \ell_d$ and $V_r \equiv V_{\ell_d}$ for $r = \ell_d$. We call V_r the *POD space* for simplicity. So far, let us point out that we have introduced the following Hilbert spaces with inclusion relations as:

$$V_r \subseteq \mathscr{V}_{\ell_d} \subset V_h \subset V \subseteq H^1(\Omega) \subset L^2(\Omega). \tag{57}$$

Remark 2 The POD modes (53) and eigenvalue truncation error (54) computed from snapshots, which are obtained from space and time discretizations, are different both from those based on snapshots obtained only from time semi-discretization, but without space discretization, as e.g. done in [19,21,27]. By using IGA, the snapshots are also different from other spatial discretizaton techniques as e.g. FEM [24,31] and Finite Volumes [32].

4 IGA-θ-POD Galerkin scheme

The POD basis can be generated by successively using the fully discrete IGA-θ method for computing the snapshots and then singular value decomposition of the correlation matrix K for obtaining the POD modes. We then use this basis to derive the POD semi-discrete scheme and IGA-θ-POD fully discrete scheme.

Given $t \in (0,T]$, the POD-Galerkin semi-discrete scheme consists in finding $u_r(t) \in V_r$ such that

$$\begin{cases} \dfrac{\mathrm{d}}{\mathrm{d}t}(u_r(t), v_r) + a(u_r(t), v_r) = (f(t), v_r) \quad \forall v_r \in V_r \\ u_r(0) = u_{0,r}, \end{cases} \tag{58}$$

where $u_{0,r}$ is the L^2-projection of $u_{0,h}$ from V_h onto V_r, the POD space of dimension r. We can define a matrix-vector form for the Galerkin POD semi-discretization:

$$\begin{cases} M_r \dot{\boldsymbol{d}}_r(t) + A_r \boldsymbol{d}_r(t) = \boldsymbol{f}_r(t), \quad t \in (0,T], \\ \boldsymbol{d}_r(0) = \boldsymbol{d}_{r,0} \end{cases} \tag{59}$$

where

$$\begin{aligned} &A_r = [a_{r,ij}] \in \mathbb{R}^{r\times r}, a_{r,ij} := a(\psi_j, \psi_i), \;\; M_r = [m_{r,ij}] \in \mathbb{R}^{r\times r}, m_{r,ij} := \int_\Omega \psi_j \psi_i \mathrm{d}x, \\ &\boldsymbol{d}_r(t) = (d_{r,1}(t), \ldots, d_{r,r}(t))^{\mathrm{T}} \in \mathbb{R}^r, \; d_{r,0} = (d_{0r,1}, \ldots, d_{0r,r})^{\mathrm{T}} \in \mathbb{R}^r, \\ &\boldsymbol{f}_r(t) = (f_{r,1}(t), \ldots, f_{r,r}(t))^{\mathrm{T}} \in \mathbb{R}^r, \; f_{r,i}(t) := \int_\Omega f(t)\psi_i \mathrm{d}x \end{aligned}$$

with $1 \le i, j \le r$.

We present now the IGA-θ-POD Galerkin fully discrete scheme for $0 \le \theta \le 1$: find $u_r^n \in V_r$, $n = 1, \ldots, N_t$ such that

$$\begin{cases} (\bar{\partial} u_r^n, v_r) + a(u_r^{n+\theta}, v_r) = (f^{n+\theta}, v_r) \quad \forall v_r \in V_r \quad n = 0, \ldots, N_t - 1 \\ u_r^0 = u_{0,r}. \end{cases} \tag{60}$$

The matrix-vector form for IGA-θ-POD Galerkin scheme reads:

$$\begin{cases} M_r \bar{\partial} \boldsymbol{d}_r^n + A_r \boldsymbol{d}_r^{n+\theta} = \boldsymbol{f}_r^{n+\theta}, \quad n = 0, \ldots, N_t - 1 \\ \boldsymbol{d}_r^0 = \boldsymbol{d}_{r,0}. \end{cases} \tag{61}$$

By solving this system, we obtain $\{d_r^n\}_{n=0}^{N_t}$ which leads to the POD Galkerin solution $\{u_r^n\}_{n=0}^{N_t}$ with $u_r^n = \sum_{j=1}^{r} d_{r,j}^n \psi_j$. The POD mass matrix M_r, POD-stiffness matrix A_r, the inverse matrices M_r^{-1} and A_r^{-1} are positive definite [27,24]. Let $\mu_1 \geq \mu_2 \geq \ldots \geq \mu_r > 0$ and $\nu_1 \geq \nu_2 \geq \ldots \geq \nu_r > 0$ be the eigenvalues of M_r and singular values of A_r, respectively; in addition, $\|\cdot\|_2$ denotes the spectral norm of a matrix. Then we have the following properties in the POD space:

Lemma 6 (Inequalities in POD space) *For all $v_r \in V_r$, we have*

$$\|v_r\|_{L^2(\Omega)} \leq \sqrt{\nu_r^{-1}\mu_1}\, \|v_r\|_{H^1(\Omega)} \quad \textit{and} \quad \|v_r\|_{H^1(\Omega)} \leq \sqrt{\mu_r^{-1}\nu_1}\, \|v_r\|_{L^2(\Omega)} \tag{62}$$

with $\nu_1 > \mu_r$. In particular,

$$\|v_r\|_{L^2(\Omega)} \leq \sqrt{\nu_r^{-1}}\, \|v_r\|_{H^1(\Omega)} \quad \textit{and} \quad \|v_r\|_{H^1(\Omega)} \leq \sqrt{\nu_1}\|v_r\|_{L^2(\Omega)} \tag{63}$$

with $\nu_1 > 1$ for POD basis in $X = L^2(\Omega)$ and

$$\|v_r\|_{L^2(\Omega)} \leq \sqrt{\mu_1}\|v_r\|_{H^1(\Omega)} \quad \textit{and} \quad \|v_r\|_{H^1(\Omega)} \leq \sqrt{\mu_r^{-1}}\, \|v_r\|_{L^2(\Omega)} \tag{64}$$

with $\mu_r < 1$ for POD basis in $X = H^1(\Omega)$.

Proof By definition of matrix 2-norm and positive definite properties of M_r, M_r^{-1}, A_r, and A_r^{-1}, we easily have

$$\|M_r\|_2 = \mu_1,\ \|M_r^{-1}\|_2 = \mu_r^{-1},\ \|A_r\|_2 = \nu_1, \text{ and } \|A_r^{-1}\|_2 = \nu_r^{-1}. \tag{65}$$

By means of (65) and Lemma 2 of [27], the inequalities (62), (63), and (64) hold.

By the second inequality of (62) and the fact that $\|v_r\|_{L^2(\Omega)} \leq \sqrt{C_\Omega}\|v_r\|_{H^1(\Omega)}$ for any $v_r \in V_r$ from (4), we obtain $C_\Omega \nu_1 \geq \mu_r$ and thus $\nu_1 > \mu_r$ since $C_\Omega \in (0,1)$. In particular, for POD basis in $L^2(\Omega)$ or $H^1(\Omega)$, the mass matrix or stiffness matrix turn out to be the identity matrix and so that $\nu_1 > 1$ or $\mu_r < 1$ follows. □

Remark 3 The second inequality of (63) (resp. (64)) is an inverse inequality in the POD space which is similar (as in Lemma 2) for both the NURBS spaces of IGA and piecewise Lagrange polynomial spaces of FEM (in Lemma 3.1 [24]). However, the values of ν_1, ν_r, μ_1 and μ_r can significantly differ depending on whether we use IGA or FEM methods.

We now show the following stability property.

Theorem 3 (IGA-θ-POD Stability) *Assume that the map $t \to \|f(t)\|_{L^2(\Omega)}$ is bounded in $[0,T]$ and $\theta \in [0,1]$. Moreover, when $0 \leq \theta < 1/2$ let the time step Δt satisfy the condition*

$$\Delta t(1+\varsigma) \leq \frac{2\alpha}{(1-2\theta)\beta^2} \tag{66}$$

with $\varsigma = \mu_r^{-1}$ or ν_1 in case of the POD basis in $X = H^1(\Omega)$ or $L^2(\Omega)$, respectively. Then, there exists a unique solution $\{u_r^n\}_{n=0}^m \subset V_r$ of problem (60). The solution $u_h^n \in V_h$ of the fully discrete problem (40) satisfies

$$\|u_r^n\|_{L^2(\Omega)} \leq C_{\theta,\alpha,\beta,T}\Big(\|u_{0,r}\|_{L^2(\Omega)} + \sup_{t\in[0,T]} \|f(t)\|_{L^2(\Omega)}\Big),\ \ n = 0,1,\ldots,N_t, \tag{67}$$

where the constant $C_{\theta,\alpha,\beta,T}$ depends on θ, α, β, and T, but is independent of h and Δt.

Proof By taking $v_r = u_r^{n+\theta}$ in (60) with $0 \le \theta \le 1$, we can easily verify that

$$\frac{1}{2}\|u_r^{n+1}\|^2_{L^2(\Omega)} - \frac{1}{2}\|u_r^n\|^2_{L^2(\Omega)} + \left(\theta - \frac{1}{2}\right)\|u_r^{n+1} - u_r^n\|^2_{L^2(\Omega)} + \Delta t\, a(u_r^{n+\theta}, u_r^{n+\theta}) = \Delta t\,(f^{n+\theta}, u_r^{n+\theta}).$$

For any function $\phi \in L^2(\Omega)$, let us define

$$\|\phi\|_{-1,r} := \sup_{0 \neq v_r \in V_r} \frac{(\phi, v_r)}{\|v_r\|_{H^1(\Omega)}}, \tag{68}$$

which is a norm in V_r and $\|\phi\|_{-1,r} \le \|\phi\|_{L^2(\Omega)}$ for each $\phi \in L^2(\Omega)$. By the coercivity of $a(\cdot,\cdot)$, we have for each $\iota \in (0,1]$ that

$$\|u_r^{n+1}\|^2_{L^2(\Omega)} - \|u_r^n\|^2_{L^2(\Omega)} + (2\theta - 1)\|u_r^{n+1} - u_r^n\|^2_{L^2(\Omega)} + 2(1-\iota)\alpha\Delta t\|u_r^{n+\theta}\|^2_{H^1(\Omega)} \le \frac{\Delta t}{2\iota\alpha}\|f^{n+\theta}\|^2_{-1,r}, \tag{69}$$

where a Young type inequality has been used. When $\theta \in [1/2, 1]$, i.e. $2\theta - 1 \ge 0$, we can set $\iota = 1$ and then

$$\|u_r^{n+1}\|^2_{L^2(\Omega)} - \|u_r^n\|^2_{L^2(\Omega)} \le \frac{\Delta t}{2\alpha}\|f^{n+\theta}\|^2_{-1,r}. \tag{70}$$

When $\theta \in [0, 1/2)$, we choose $v_r = u_r^{n+1} - u_r^n$ in (60) and obtain

$$\begin{aligned}\|u_r^{n+1} - u_r^n\|^2_{L^2(\Omega)} &= -\Delta t\, a(u_r^{n+\theta}, u_r^{n+1} - u_r^n) + \Delta t(f^{n+\theta}, u_r^{n+1} - u_r^n)\\ &\le \beta\Delta t\|u_r^{n+\theta}\|_{H^1(\Omega)}\|u_r^{n+1} - u_r^n\|_{H^1(\Omega)}\\ &\quad + \Delta t\|f^{n+\theta}\|_{-1,r}\|u_r^{n+1} - u_r^n\|_{H^1(\Omega)}.\end{aligned}$$

In virtue of the POD inverse inequalities (63) and (64), we have

$$\|u_r^{n+1} - u_r^n\|_{L^2(\Omega)} \le \Delta t(1+\varsigma)^{1/2}(\beta\|u_r^{n+\theta}\|_{H^1(\Omega)} + \|f^{n+\theta}\|_{-1,r}), \tag{71}$$

where $\varsigma = \mu_r^{-1}$ or ν_1 for the POD basis associated with $X = H^1(\Omega)$ or $L^2(\Omega)$, respectively. For each $\gamma > 0$, we define $\kappa_\gamma := 2(1-\iota)\alpha - (1-2\theta)\beta(\beta+\gamma)\Delta t(1+\varsigma)$. It follows from (69) and (71) that there exists a positive constant $C_{\iota,\gamma}$ dependent on ι and γ such that

$$\|u_r^{n+1}\|^2_{L^2(\Omega)} - \|u_r^n\|^2_{L^2(\Omega)} + \Delta t\,\kappa_\gamma\|u_r^{n+\theta}\|^2_{H^1(\Omega)} \le C_{\iota,\gamma}\Delta t(1+\Delta t\varsigma)\|f^{n+\theta}\|^2_{-1,r}. \tag{72}$$

Specifically, we choose ι and γ sufficiently small such that we have $\kappa_\gamma > 0$ due to (66). From (66), we also have $1 + \Delta t\,\varsigma \le C_{\theta,\alpha,\beta}$ with the constant $C_{\theta,\alpha,\beta}$ depending on θ, α and β. Therefore, we obtain from (72)

$$\|u_r^{n+1}\|^2_{L^2(\Omega)} - \|u_r^n\|^2_{L^2(\Omega)} \le C_{\iota,\gamma}C_{\theta,\alpha,\beta}\,\Delta t\|f^{n+\theta}\|^2_{-1,r}. \tag{73}$$

For a fixed integer index m, $1 \le m \le N_t$, we consider both the cases $\theta \in [0, 1/2)$ and $[1/2, 1]$. We sum up for both (70) and (73) from $n = 0, \ldots, m-1$ and then we find

$$\|u_r^m\|^2_{L^2(\Omega)} \le \|u_{0,r}\|^2_{L^2(\Omega)} + C_{\iota,\gamma}C_{\theta,\alpha,\beta}\,\Delta t\sum_{n=0}^{N_t-1}\|f^{n+\theta}\|^2_{-1,r}, \tag{74}$$

from which we easily obtain (67). □

4.1 *A priori* error estimates of IGA-θ-POD Galerkin scheme

Before studying the convergence property of the IGA-θ-POD Galerkin scheme, we first define an *elliptic "projection" operator* $\mathscr{P}_{h,r}: V_h \to V_r$ for any $u_h \in V_h$ as

$$a(\mathscr{P}_{h,r}u_h, v_r) = a(u_h, v_r) \quad \forall v_r \in V_r. \tag{75}$$

The problem (75) is well posed in virtue of the Lax-Milgram theorem due to properties (6) and (7). Moreover,

$$\|\mathscr{P}_{h,r}u_h\|_{H^1(\Omega)} \le \frac{\beta}{\alpha}\|u_h\|_{H^1(\Omega)} \quad \forall v_h \in V_h. \tag{76}$$

Then, we obtain the following error estimates for the projection errors.

Lemma 7 *For every $r \in \{1,\dots,\ell_d\}$, the projection operators $\mathscr{P}_{h,r}$ yields the following bounds on the projection errors for $X = L^2(\Omega)$:*

$$\frac{1}{N_t}\sum_{n=1}^{N_t}\|u_h^n - \mathscr{P}_{h,r}u_h^n\|_{H^1(\Omega)}^2 \le \frac{3\beta^2\nu_1}{\alpha^2}\sum_{k=r+1}^{\ell_d}\hat{\lambda}_k, \tag{77}$$

$$\frac{1}{N_t}\sum_{n=0}^{N_t-1}\|\bar{\partial}u_h^n - \mathscr{P}_{h,r}(\bar{\partial}u_h^n)\|_{H^1(\Omega)}^2 \le \frac{3\beta^2\nu_1}{\alpha^2}\sum_{k=r+1}^{\ell_d}\hat{\lambda}_k, \tag{78}$$

and for $X = H^1(\Omega)$:

$$\frac{1}{N_t}\sum_{n=1}^{N_t}\|u_h^n - \mathscr{P}_{h,r}u_h^n\|_{H^1(\Omega)}^2 \le \frac{3\beta^2}{\alpha^2}\sum_{k=r+1}^{\ell_d}\tilde{\lambda}_k, \tag{79}$$

$$\frac{1}{N_t}\sum_{n=0}^{N_t-1}\|\bar{\partial}u_h^n - \mathscr{P}_{h,r}(\bar{\partial}u_h^n)\|_{H^1(\Omega)}^2 \le \frac{3\beta^2}{\alpha^2}\sum_{k=r+1}^{\ell_d}\tilde{\lambda}_k. \tag{80}$$

Proof For any $u_h \in \mathscr{V}_{\ell_d}$, we have from (75) that

$$\begin{aligned}\alpha\|u_h - \mathscr{P}_{h,r}u_h\|_{H^1(\Omega)}^2 &\le a(u_h - \mathscr{P}_{h,r}u_h, u_h - \mathscr{P}_{h,r}u_h)\\ &= a(u_h - \mathscr{P}_{h,r}u_h, u_h - v_r)\\ &\le \beta\|u_h - \mathscr{P}_{h,r}u_h\|_{H^1(\Omega)}\|u_h - v_r\|_{H^1(\Omega)} \quad \forall v_r \in V_r,\end{aligned}$$

which implies that

$$\|u_h - \mathscr{P}_{h,r}u_h\|_{H^1(\Omega)} \le \frac{\beta}{\alpha}\|u_h - v_r\|_{H^1(\Omega)} \quad \forall v_r \in V_r. \tag{81}$$

The results then follow similarly to Lemma 3 and Corollary 4 in [27] by using a combination of (55), (56), Lemma 6, and (81). □

Remark 4 We remark that the above results have been obtained by using the projection operator $\mathscr{P}_{h,r}: V_h \to V_r$, which is different from the one typically used in the POD literature and is defined from V to V_r [24,27]. Our choice is motivated by the fact that the projector $\mathscr{P}_{h,r}$ serves for the analysis of the error $u_h^n - u_r^n$.

We remark that the error bounds of the IGA-θ-POD Galerkin scheme include three components arising from IGA space discretization, time discretization and POD eigenvalue truncation.

Theorem 4 *Let the assumptions in Theorem 1, Lemmas 4 and 5 hold. Moreover, we assume that (66) in Theorem 3 holds when $\theta \in [0,1/2)$. Then, for the IGA-θ-POD Galerkin scheme with $\theta \in [0,1]$, we have*

$$\frac{1}{N_t}\sum_{n=1}^{N_t}\|u^n-u_r^n\|_{L^2(\Omega)}^2 \le C\left(\|u_r^0-\mathscr{P}_{h,r}u_h^0\|_{L^2(\Omega)}^2+\Delta t^{2\vartheta(\theta)}+h^{2(p+1)}+\sum_{k=r+1}^{\ell_d}\lambda_k\right) \tag{82}$$

with $\vartheta(\theta)=2$ for $\theta=1/2$, and $\vartheta(\theta)=1$ for $\theta\neq 1/2$, the constant $C=C(\alpha,\beta,\theta,\Omega,C_\Omega,\|\nabla \boldsymbol{F}\|_{L^\infty(\hat{\Omega})},k_{\mathrm{m}},\nu_1)>0$ independent of Δt, h, p, and $\lambda_k=\hat{\lambda}_k$ for $X=L^2(\Omega)$, while $C=C(\alpha,\beta,\theta,\Omega,C_\Omega,\|\nabla \boldsymbol{F}\|_{L^\infty(\hat{\Omega})},k_{\mathrm{m}})$ with $\lambda_k=\tilde{\lambda}_k$ for $X=H^1(\Omega)$.

Proof Since $u^n-u_r^n=(u^n-u_h^n)+(u_h^n-u_r^n)$, we have by the triangle inequality

$$\|u^n-u_r^n\|_{L^2(\Omega)} \le \|u^n-u_h^n\|_{L^2(\Omega)}+\|u_h^n-u_r^n\|_{L^2(\Omega)}. \tag{83}$$

The first term on the right hand side of (83) is bounded via the IGA fully-discrete error estimation in Theorem 2. We write (46) and (47) as a unified error estimator for simplicity, for which:

$$\|u^n-u_h^n\|_{L^2(\Omega)} \le \bar{C}^*(h^{p+1}+\Delta t^{\vartheta(\theta)}), \quad \theta\in[0,1] \tag{84}$$

for a positive constant $\bar{C}^*=\bar{C}^*(\Omega,\alpha,\beta,\theta,T,k_{\mathrm{m}})$ independent of Δt and h. To estimate the second term of (83), we write

$$\begin{aligned} u_h^n-u_r^n &= (u_h^n-\mathscr{P}_{h,r}u_h^n)+(\mathscr{P}_{h,r}u_h^n-u_r^n)\\ &\equiv \eta^n+\rho_r^n, \end{aligned}$$

where $\eta^n := u_h^n-\mathscr{P}_{h,r}u_h^n$ and $\rho_r^n := \mathscr{P}_{h,r}u_h^n-u_r^n$. From (79) and (77) of Lemma 7, we have for η^n the average square error

$$\begin{aligned} \frac{1}{N_t}\sum_{n=1}^{N_t}\|\eta^n\|_{L^2(\Omega)}^2 &\le \frac{C_\Omega}{N_t}\sum_{n=1}^{N_t}\|\eta^n\|_{H^1(\Omega)}^2\\ &\le \frac{3\beta^2C_\Omega\nu_1}{\alpha^2}\sum_{i=r+1}^{\ell_d}\hat{\lambda}_i \quad \text{for } X=L^2(\Omega)\\ &\text{or } \frac{3\beta^2C_\Omega}{\alpha^2}\sum_{i=r+1}^{\ell_d}\tilde{\lambda}_i \quad \text{for } X=H^1(\Omega). \end{aligned} \tag{85}$$

By (75), (40), and the fact that the linear operator $\bar{\partial}$ commutes with $\mathscr{P}_{h,r}$, we can write

$$\begin{aligned} (\bar{\partial}\rho_r^n,v_r)+a(\rho_r^{n+\theta},v_r) &= (\bar{\partial}(\mathscr{P}_{h,r}u_h^n),v_r)+a(\mathscr{P}_{h,r}(u_h^{n+\theta}),v_r)-(\bar{\partial}u_r^n,v_r)-a(u_r^{n+\theta},v_r)\\ &= (\mathscr{P}_{h,r}(\bar{\partial}u_h^n),v_r)+a(u_h^{n+\theta},v_r)-(f^{n+\theta},v_r)\\ &= (\mathscr{P}_{h,r}(\bar{\partial}u_h^n),v_r)-(\bar{\partial}u_h^n,v_r)\equiv(z_r^n,v_r) \qquad \forall v_r\in V_r, \end{aligned} \tag{86}$$

where $z_r^n := \mathscr{P}_{h,r}(\bar{\partial}u_h^n)-\bar{\partial}u_h^n$.

We now bound $\|\rho^n\|_{L^2(\Omega)}$ by $\|z^n\|_{L^2(\Omega)}$. By taking $v_r=\rho_r^{n+\theta}$ in the last equality of (86), we can easily verify that

$$\begin{aligned} \frac{1}{2}\|\rho_r^{n+1}\|_{L^2(\Omega)}^2-\frac{1}{2}\|\rho_r^n\|_{L^2(\Omega)}^2+\left(\theta-\frac{1}{2}\right)\|\rho_r^{n+1}-\rho_r^n\|_{L^2(\Omega)}^2\\ +\Delta t\,a(\rho_r^{n+\theta},\rho_r^{n+\theta})=\Delta t(z_r^n,\rho_r^{n+\theta}). \end{aligned}$$

Then, we consider separately the cases $\theta \in [0,1/2)$ and $\theta \in [1/2,1]$ and use a similar proof for the stability as in Theorem 3, yielding

$$\|\rho_r^m\|_{L^2(\Omega)}^2 \leq \|\rho_r^0\|_{L^2(\Omega)}^2 + C^* \Delta t \sum_{n=0}^{m-1} \|z_r^n\|_{L^2(\Omega)}^2, \quad m = 1,\ldots,N_t \tag{87}$$

with $C^* = C^*(\alpha,\beta,\theta,T)$. Hence, we sum up from $m=1$ to N_t for (87) and we obtain

$$\begin{aligned}
\frac{1}{N_t}\sum_{m=1}^{N_t} \|\rho_r^m\|_{L^2(\Omega)}^2 &\leq \|\rho_r^0\|_{L^2(\Omega)}^2 + C^* \frac{\Delta t}{N_t} \sum_{m=1}^{N_t}\sum_{n=0}^{m-1} \|z_r^n\|_{L^2(\Omega)}^2 \\
&\leq \|\rho_r^0\|_{L^2(\Omega)}^2 + C^* \frac{\Delta t}{N_t} N_t \sum_{n=0}^{N_t-1} \|z_r^n\|_{L^2(\Omega)}^2. \\
&= \|\rho_r^0\|_{L^2(\Omega)}^2 + \frac{C^* T}{N_t} \sum_{n=0}^{N_t-1} \|z_r^n\|_{L^2(\Omega)}^2.
\end{aligned} \tag{88}$$

By means of (80) and (78) of Lemma 7, we have

$$\begin{aligned}
\frac{1}{N_t}\sum_{n=0}^{N_t-1} \|z_r^n\|_{L^2(\Omega)}^2 &= \frac{1}{N_t}\sum_{n=0}^{N_t-1} \|\mathscr{P}_{h,r}\bar{\partial} u_h^n - \bar{\partial} u_h^n\|_{L^2(\Omega)}^2 \\
&\leq \frac{3\beta^2 C_\Omega \nu_1}{\alpha^2} \sum_{k=r+1}^{\ell_d} \hat{\lambda}_k \quad \text{for } X = L^2(\Omega) \\
&\text{or } \frac{3\beta^2 C_\Omega}{\alpha^2} \sum_{k=r+1}^{\ell_d} \tilde{\lambda}_k \quad \text{for } X = H^1(\Omega).
\end{aligned} \tag{89}$$

Therefore, we have from (88) and (89)

$$\begin{aligned}
\frac{1}{N_t}\sum_{n=1}^{N_t} \|\rho_r^n\|_{L^2(\Omega)}^2 &\leq \|\rho_r^0\|_{L^2(\Omega)}^2 + C^{**}\nu_1 \sum_{k=r+1}^{\ell_d} \hat{\lambda}_k \quad \text{for } X = L^2(\Omega) \\
&\text{or } \|\rho_r^0\|_{L^2(\Omega)}^2 + C^{**} \sum_{k=r+1}^{\ell_d} \tilde{\lambda}_k \quad \text{for } X = H^1(\Omega).
\end{aligned} \tag{90}$$

with $C^{**} = C^{**}(\alpha,\beta,\theta,T,C_\Omega)$. A combination of (90) with (85) and (84) implies that (82). □

Remark 5 We can estimate $\|u_r^0 - \mathscr{P}_{h,r}u_h^0\|_{L^2(\Omega)}$ since the initial data is included in the set of snapshots, i.e. $u_h^0 \in V_r$. From (4), (81) and (56) (resp. (55)), we have

$$\begin{aligned}
\|u_h^0 - \mathscr{P}_{h,r}u_h^0\|_{L^2(\Omega)}^2 &\leq \frac{C_\Omega \beta^2}{\alpha^2} \left\| u_r^0 - \sum_{k=1}^{r} (u_h^0, \psi_k)_X \, \psi_k \right\|_{H^1(\Omega)}^2 \\
&\leq N_s \frac{C_\Omega \beta^2 \nu_1}{\alpha^2} \sum_{k=r+1}^{\ell_d} \hat{\lambda}_k \quad \text{for } X = L^2(\Omega) \\
&\text{or } N_s \frac{C_\Omega \beta^2}{\alpha^2} \sum_{k=r+1}^{\ell_d} \tilde{\lambda}_k \quad \text{for } X = H^1(\Omega)
\end{aligned}$$

Therefore, if we choose $r = \ell_d$, (82) reduces to

$$\frac{1}{N_t}\sum_{n=1}^{N_t} \|u^n - u_r^n\|_{L^2(\Omega)}^2 \leq C\left(\Delta t^{2\vartheta(\theta)} + h^{2(p+1)}\right).$$

4.2 Numerical aspects

We present the full IGA-θ-POD Galerkin method for model order reduction in `Algorithm` 1 which contains three modules: the snapshot computation by IGA, the POD basis generation and the POD-θ Galerkin approach. Let us denote a diagonal matrix $\Theta = \mathrm{diag}(\alpha_1, \ldots, \alpha_{N_s})$. In `Algorithm` 1, we consider three approaches to generate POD basis as suggested in [44]. They are mathematically equivalent for modal analysis, although their computational costs are generally different. The correlation matrix (52) and POD basis (54) correspond to Case 3.

The choice of the POD rank r is crucial since it influences the accuracy of the POD reduced order modeling in approximating the original problem. In our IGA-θ-POD-Galerkin method, we can determine r also based on a heuristic rule [44]. More precisely, given an error tolerance ε $(0 < \varepsilon \ll 1)$, we determine r such that the computed energy ratio

$$E(r) := \frac{\sum_{i=1}^{r} \lambda_i}{\sum_{i=1}^{\ell_d} \lambda_i} > 1 - \varepsilon, \tag{91}$$

or equivalently,

$$1 - E(r) = \frac{\sum_{i=r+1}^{\ell_d} \lambda_i}{\mathrm{trace}(D^{\mathrm{T}} D)} < \varepsilon \tag{92}$$

The time and spatial discretizations have direct effects on the correlation matrix and thus on the eigenvalues. More precisely, the parameters θ, Δt, p, k_{m} and h influence the accuracy of $\{\lambda_i\}_{i=1}^{d}$. Moreover, the choice of the weight matrix W (i.e. $W = M$ or $W = M + A$ for $X = L^2(\Omega)$ or $H^1(\Omega)$, respectively) and the inclusion of TDQ (i.e. $N_s = 2N_t + 1$ or $N_s = N_t + 1$) can additionally affect the eigenvalue analysis. Once the eigenvalues have been computed however, we find from (92) that a POD rank r only directly depends on ε. The smaller is ε, the larger is r, which leads to more accurate approximations of the POD Galerkin solutions to snapshots.

Once the POD rank and POD basis have been determined, we set

$$\Psi = [\psi_1 | \ldots | \psi_r] \in \mathbb{R}^{N_x \times r}.$$

Then, we obtain for (61):

$$M_r = \Psi^{\mathrm{T}} M \Psi, \quad A_r = \Psi^{\mathrm{T}} A \Psi, \quad \boldsymbol{f}_r^n = \Psi^{\mathrm{T}} \boldsymbol{f}^n \ \text{ for } n = 1, \ldots, N_t.$$

Given θ, we compute $\boldsymbol{d}_r^n$ by solving (61) and obtain $u_r^n = \Psi \boldsymbol{d}_r^n$.

5 Numerical tests

In this section, we show numerical comparisons between the IGA-θ-POD Galerkin method and the FEM-θ-POD Galerkin method and highlight the advantages of the former approach both in terms of efficiency and accuracy. Specifically, for the two POD-Galerkin methods, we compare IGA with FEM spatial discretization and study the influence of this choice on POD eigenpairs and the accuracy of POD solutions. Clearly, there is no obvious difference between the two methods for the time discretization error when the same θ-scheme and Δt are used. In order to focus on comparing the two methods on space discretization and POD truncation, we use in the following the same Crank-Nicolson scheme ($\theta = 1/2$) and assume that the error due to time discretization is relatively "small" compared with the two error

Algorithm 1 IGA-θ-POD Galerkin method for model order reduction of parabolic PDEs

procedure SNAPSHOTS(Method of snapshots based on IGA-θ-scheme)
Require: Set θ, Δt, $N_s = 2[T/\Delta t]+1$ (or $[T/\Delta t]+1$) if TDQ are included (or not), p, $k_{\rm m}$, N_x, and ε;
    Solve PDE by the full discrete IGA-θ Galerkin scheme to obtain snapshots $\{\boldsymbol{d}_h^n\}_{n=0}^{N_s} \subset \mathbb{R}^{N_x}$;
return $D = \left[\boldsymbol{d}_h^1 | \ldots | \boldsymbol{d}_h^{N_s}\right] \in \mathbb{R}^{N_x \times N_s}$;
procedure POD(POD basis of rank r)
Require: Weight matrix W, diagonal matrix Θ for temporal quadrature weights;
Case 1: if $N_x = N_s$
    Compute $\bar{D} = W^{1/2} D \Theta^{1/2}$;
    Perform singular value decomposition: $\bar{D} = \bar{\Psi} \Sigma \bar{\Phi}^{\rm T}$;
    Determine POD rank r;
    Compute $\psi_i = W^{-1/2} \bar{\Psi}_i \in \mathbb{R}^{N_x}$ and set $\lambda_i = \Sigma_{ii}^2$ for $i = 1, \ldots, r$;
Case 2: if $N_x < N_s$
    Compute $\bar{D} = W^{1/2} D \Theta^{1/2}$;
    Compute $R = \bar{D}\bar{D}^{\rm T} \in \mathbb{R}^{N_x \times N_x}$;
    Perform eigenvalue decomposition: $R = \bar{\Psi} \Lambda \bar{\Psi}^{\rm T}$;
    Determine POD rank r;
    Compute $\psi_i = W^{-1/2} \bar{\Psi}_i \in \mathbb{R}^{N_x}$ and set $\lambda_i = \Lambda_{ii}$ for $i = 1, \ldots, r$;
Case 3: if $N_x > N_s$
    Compute $K = \Theta^{1/2} D^{\rm T} W D \Theta^{1/2} \in \mathbb{R}^{N_s \times N_s}$;
    Perform eigenvalue decomposition: $K = \bar{\Phi} \Lambda \bar{\Phi}^{\rm T}$;
    Determine POD rank r;
    Compute $\psi_i = D\Theta^{1/2} \bar{\Phi}_i / \sqrt{\lambda_i} \in \mathbb{R}^{N_x}$ and set $\lambda_i = \Lambda_{ii}, i = 1, \ldots, r$;
return IGA-POD basis $\{\psi_i\}_{i=1}^r$ and eigenvalues $\{\lambda_i^h\}_{i=1}^r$.
procedure POD GALERKIN SCHEME(Model Order Reduction)
Require:
    Solve PDE by the full discrete POD-θ-scheme (61) to obtain POD basis coefficients $\{\boldsymbol{d}_r^n\}_{n=0}^{N_t} \subset \mathbb{R}^r$;
    Compute $u_r^n = \sum_{j=1}^r (\boldsymbol{d}_r^n)_j \psi_j$ for $n = 0, \ldots, N_t$;
return POD Galerkin solutions $\{u_r^n\}_{n=0}^{N_t}$.

components due to space discretization and POD projection, i.e. $\Delta t^2 \ll h^{p+1}$ (or h^p) for L^2-norm (or H^1-norm) and $\Delta t^2 \ll \sqrt{\varepsilon}$. For the error due to space discretization, however, IGA is expected to be more accurate than FEM at least when approximating smooth solutions. More precisely, NURBS of IGA can have regularity up to C^{p-1}, higher than the C^0-continuity of piecewise Lagrange polynomials used in FEM. Moreover, IGA can improve accuracy of numerical solutions by performing h-p-k refinements, while h-p refinement can only be used in FEM. Finally, IGA facilitates the exact geometrical representation of computational domains, as conic sections, in the analysis conversely to FEM. The spatial discretization is carried out by means of NURBS-based IGA with piecewise B-splines of degree $p = 2$ and the smoothness parameter $k_{\rm m} = 0, 1$. The k-refinement is performed by order elevation from $p = 1$ and knot insertion. For the comparison, we use FEM with $p = 2$, the degree of C^0-continuous piecewise Lagrange polynomials. For the generation of POD basis, we consider the choices of $X = H^1(\Omega)$ or $L^2(\Omega)$, eventually including TDQ.

Let us first introduce some notations about numerical errors we use for performing the comparison. The discrete average error norm for the IGA/FEM-θ-POD model order reduction is assessed by

$$\mathscr{E}_{r,Z} := \frac{1}{N_t+1} \sum_{n=0}^{N_t} \|u^n - u_r^n\|_Z, \tag{93}$$

where Z denotes $L^2(\Omega)$ or $H^1(\Omega)$ and u_r^n denotes the POD-Galerkin solution at t_n associated with IGA or FEM discretizations. Let us denote by $\mathscr{E}_Z$ and $\mathscr{E}_Z^{s,r}$ the two error parts splitting

$\mathscr{E}_{r,Z}$ as in (1), respectively:

$$\mathscr{E}_Z := \frac{1}{N_t+1}\sum_{n=0}^{N_t}\|u^n-u_h^n\|_Z \quad \text{and} \quad \mathscr{E}_Z^{s,r} := \frac{1}{N_t+1}\sum_{n=0}^{N_t}\|u_h^n-u_r^n\|_Z, \tag{94}$$

We then have

$$\mathscr{E}_{r,Z} \le \mathscr{E}_Z + \mathscr{E}_Z^{s,r}. \tag{95}$$

This type of norm $\mathscr{E}_{r,Z}$, also adopted in [24,30] associated with FEM, can actually be sharply bounded by the discrete average norm [24]:

$$\mathscr{E}_{r,Z} \le \left(\frac{1}{N_t+1}\sum_{n=0}^{N_t}\|u^n-u_r^n\|_Z^2\right)^{1/2}. \tag{96}$$

By using (96), Theorem 4 and (91), the expected error bound $\mathscr{E}_{r,L^2}$ (resp. $\mathscr{E}_{r,H^1}$) should be $\mathscr{O}(\Delta t^2+h^3+\sqrt{\varepsilon})$ (resp. $\mathscr{O}(\Delta t^2+h^2+\sqrt{\varepsilon})$).

Example 5.1

We consider the heat equation in an annulus $\Omega = \{(\rho,\theta)|1<\rho<2, 0<\theta<\pi/2\}$ as example. We set $T=4$ and $\Delta t = 2\times 10^{-3}$, for which $\mathscr{O}(\Delta t^2)=\mathscr{O}(10^{-6})$. Choose the exact solution

$$u(x_1,x_2,t) = \mathrm{e}^{-\frac{t}{4}}\sin\left(\frac{\pi}{10}(2x_1^2+x_2^2)(t+2)\right)$$

and compute the corresponding source function f, boundary conditions, and initial condition according with Eq. (3) by setting in Eq. (2) $a_0=0$, $\tilde{a}_{ij}=\delta_{ij}$, $b_i=0$ and $c_i=0$ for $i,j=1,2$. Specifically, we impose Neumann boundary conditions on $\Gamma_N=\Gamma_{N_0}\cup\Gamma_{N_1}\cup\Gamma_{N_2}$ and Dirichlet boundary conditions on $\Gamma_D=\partial\Omega\setminus\Gamma_N$ as shown in Fig. 2(a), where a rather coarse tensor-product NURBS mesh is reported. In Fig. 2(b), we plot for FEM a triangular mesh, which induces a geometrical approximation error. We show visually agreement between the exact solution in Fig. 2(c) and the IGA-θ-POD Galerkin solution in Fig. 2(d) at the final time.

We now compare the convergence rate and accuracy of IGA and FEM spatial discretizations. First, we check the convergence rates for errors of snapshots with respect to mesh parameters. For meshes used in IGA, we initialize the number of mesh elements as $8\times 8=64$. We remark that NURBS allows an exact representation of Ω already at the coarsest level of discretization. We then use h-refinement three times up to an element number $64\times 64 = 4{,}096$. The mesh sizes are $h=0.207$, 0.105, 0.053, and 0.026. Figs. 3(a)-3(b) show that the convergence rates for errors of snapshots by IGA $p=2$ NURBS basis functions with $k_\mathrm{m}=0$ or 1 in both of $\mathscr{E}_{L^2}$ and $\mathscr{E}_{H^1}$ norms, i.e. they are optimal with respect to NURBS-based spatial discretization (i.e. cubic and quadratic convergence rates for L^2- and H^1-norm, respectively). Conversely, Fig. 3(c) shows that the convergence rate of the error $\mathscr{E}_{L^2}$ is sub-optimal for FEM, although it appears to be optimal for that of error in H^1-norm. This is due to the fact that the approximate representation of the annular geometry causes a geometric approximation error of order 2 in h. Then, we compare IGA with FEM on the accuracy of truth approximation due to spatial discretization. We use three different levels of number of degrees of freedom (ndofs) for comparison. Table 1 shows that the truth approximations by IGA are more accurate than those by FEM, even if nearly the same or less ndofs are used. Besides, the numerical solutions for the case $k_\mathrm{m}=1$ are more accurate than

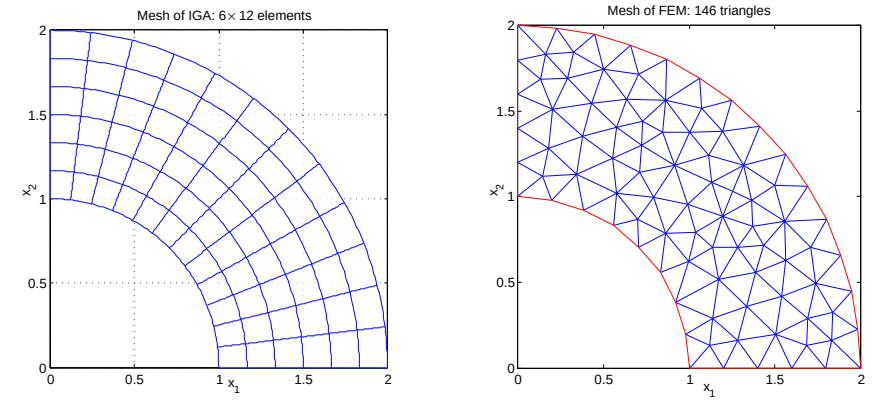

(a) IGA mesh

(b) FEM mesh

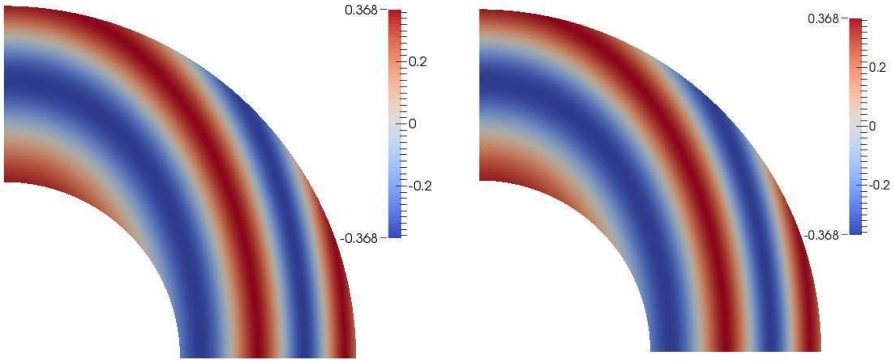

(c) Exact solution at final time

(d) IGA-θ-POD Galerkin solution

Fig. 2 Comparison between IGA and FEM on geometric representation (first row) and comparison between exact solution and POD-Galerkin solution (second row) for Example 5.1: (a) A NURBS mesh of Ω for IGA, (b) A triangular mesh of Ω for FEM, (c) Exact solution in Ω at final time, and (d) IGA-based POD Galerkin solution at final time ($k_{\rm m} = 1$, 32×32 elements, $\varepsilon = 10^{-8}$, TDQ included and $X = H^1(\Omega)$).

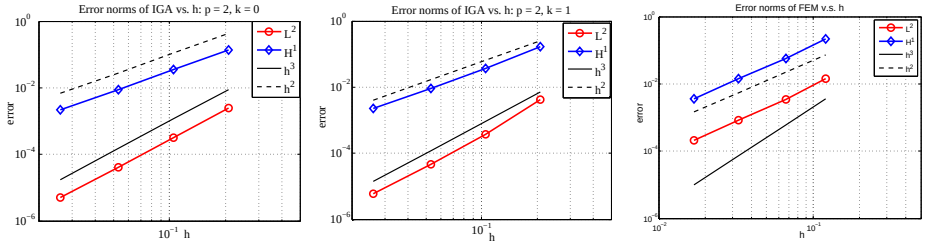

Fig. 3 Comparisons between IGA and FEM on converge rates for errors of snapshots $\mathscr{E}_{L^2}$ and $\mathscr{E}_{H^1}$ of Example 5.1.

those for $k_{\rm m} = 0$ though slightly less ndofs are used. Moreover, the accuracy of truth approximation leads to different decay behaviors for POD eigenvalues as shown in Figs. 4-5. More precisely, with nearly the same ndofs, both the figures show that IGA-based POD eigenvalues decay faster than FEM-based ones and the POD eigenvalues of IGA with $k_{\rm m} = 1$ NURBS basis decay faster than those associated to IGA with $k_{\rm m} = 0$. Roughly speaking,

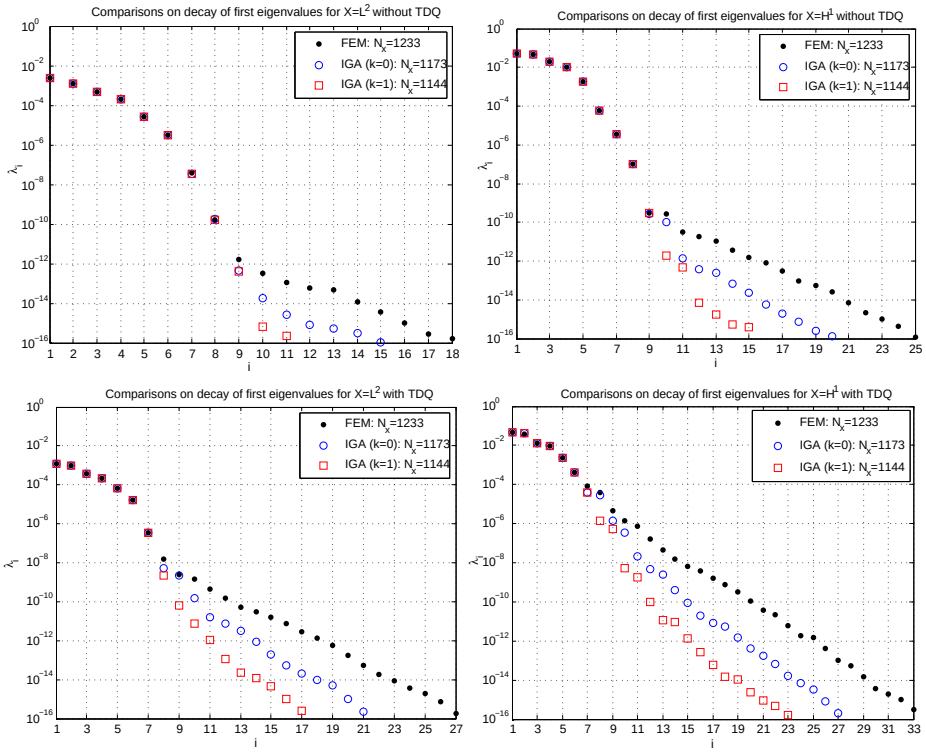

Fig. 4 Comparisons of λ_i vs. i for the IGA-θ-POD Galerkin method and FEM-θ-POD Galerkin method applied to Example 5.1: $N_x = 1{,}173$, 1,144 and 1,233 for IGA-$k_{\mathrm{m}} = 0$, IGA-$k_{\mathrm{m}} = 1$, and FEM, respectively.

these phenomenons illustrate that the POD rank r of either the two IGA cases is nearly the same as that of the FEM case, when a relatively "large" truncation error tolerance ε is used in inequality (91). Moreover, if ε is "small", the POD ranks of the two IGA cases are smaller than that of FEM and the value r of IGA $k_{\mathrm{m}} = 1$ is smaller than that of IGA $k_{\mathrm{m}} = 0$. Since smaller r means more efficient in POD-Galerkin methods for reduced order model, the IGA case with $k_{\mathrm{m}} = 1$ appears to be the most efficient, while the FEM case is the slowest among the three candidates for model reduction. We also see from these figures that the difference for eigenvalues appears earlier in the eigenvalue index i for the case including TDQ than that without it, as well as for the case with $X = H^1(\Omega)$ than that with $X = L^2(\Omega)$. Fig. 6 clearly shows what we have drawn from Figs. 4-5. We see that r increases monotonically as ε decreases. More importantly, we see that the values of r for the IGA cases are smaller than that for FEM if the same value of ε is used, which implies more efficiency for the POD-Galerkin method for the reduced order model.

With nearly the same ndofs, Table 2 shows that, whether including TDQ or not, the average discrete L^2 errors $\mathscr{E}_{L^2}^{s,r}$ between POD-Galerkin solutions and IGA-based snapshots are much smaller than those between POD-Galerkin solutions and FEM-based ones, which exhibits the advantages of using IGA in model order reduction. We compute and compare POD truncation error bounds $\sum_{i=r+1}^{\ell_d} \lambda_i$ in Table 3 for $X = L^2(\Omega)$ or $H^1(\Omega)$ and with or without TDQ. As ε decreases, these bounds decrease since r increases correspondingly. In

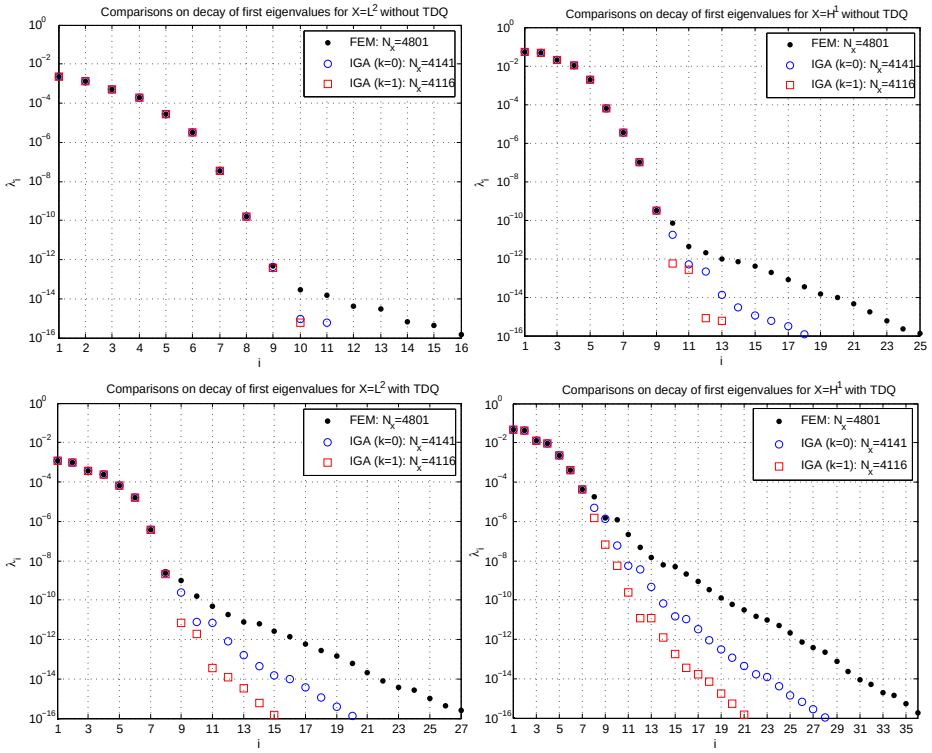

Fig. 5 Comparisons of λ_i vs. i for the IGA-θ-POD Galerkin method and FEM-θ-POD Galerkin method applied to Example 5.1: $N_x = 4,141$, 4,116 and 4,801 for IGA $k_{\mathrm{m}} = 0$, IGA $k_{\mathrm{m}} = 1$ and FEM, respectively.

Table 1 Comparisons on errors of truth approximations $\mathscr{E}_{L^2}$ and $\mathscr{E}_{H^1}$ for Example 5.1.

FEM			IGA $k_{\mathrm{m}} = 0$			IGA $k_{\mathrm{m}} = 1$		
N_x	$\mathscr{E}_{L^2}$	$\mathscr{E}_{H^1}$	N_x	$\mathscr{E}_{L^2}$	$\mathscr{E}_{H^1}$	N_x	$\mathscr{E}_{L^2}$	$\mathscr{E}_{H^1}$
325	1.92e-2	2.73e-1	325	5.08e-3	2.39e-1	324	1.57e-3	9.82e-2
1,233	4.48e-3	7.16e-2	1,173	8.52e-4	7.58e-2	1,144	1.58e-4	2.29e-2
4,801	1.09e-3	1.82e-2	4,141	1.43e-4	2.22e-2	4,116	1.84e-5	5.61e-3

most cases, the bounds of two IGA cases are smaller than those of FEM and the ones of the IGA $k_{\mathrm{m}} = 1$ case are smaller than those of the IGA $k_{\mathrm{m}} = 0$ case.

Example 5.2

We consider an unsteady advection-diffusion-reaction equation in a unit square $\Omega = (0,1)^2$ ([24]) as our second test example. In this case, we aim at addressing the use of smooth NURBS (B-splines) basis functions rather than the geometric representation of Ω. We set $T = 1$ and $\Delta t = 10^{-3}$. We choose the exact solution

$$u(x_1,x_2,t) = 0.5\sin(\pi x_1)\sin(\pi x_2)[\tanh(25(x_1+x_2-t-0.5))+1]$$

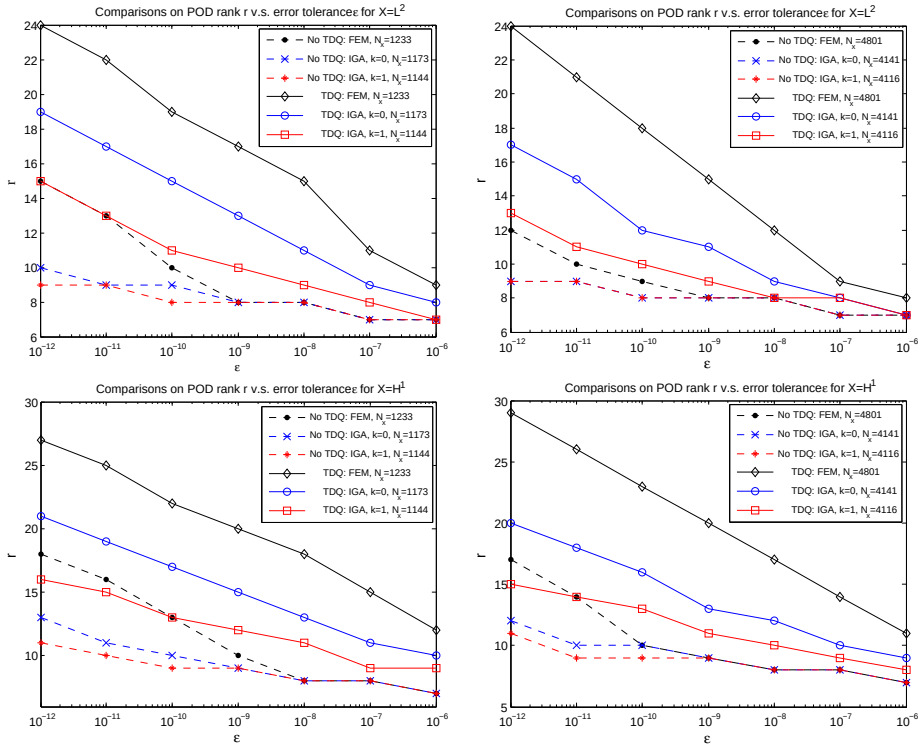

Fig. 6 Comparisons on POD rank v.s. ε obtained in $X = L^2(\Omega)/H^1(\Omega)$ and with/without TDQ for Example 5.1.

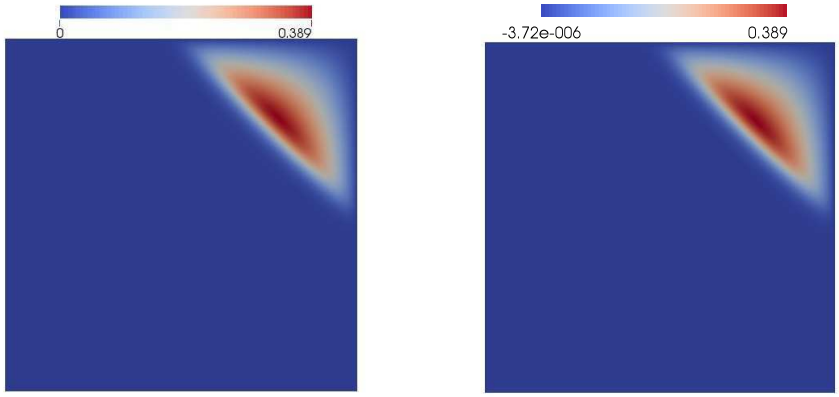

(a) (b)

Fig. 7 Comparison on exact solution at final time (a) and a IGA-θ-POD Galerkin solution (b) for Example 5.2 ($\varepsilon = 10^{-6}$, TDQ included and $X = H^1(\Omega)$).

satisfying homogeneous Dirichlet boundary condition. We set $a_0 = 1$, $\tilde{a}_{ij} = \varepsilon\delta_{ij}$, $b_i = 0$ for $i, j = 1, 2$, $c_1 = \cos(\pi/3)$ and $c_2 = \sin(\pi/3)$. We compute the corresponding f and initial condition via Eq. (3). For IGA, we use $p = 2$ with $k_{\mathrm{m}} = 1$.

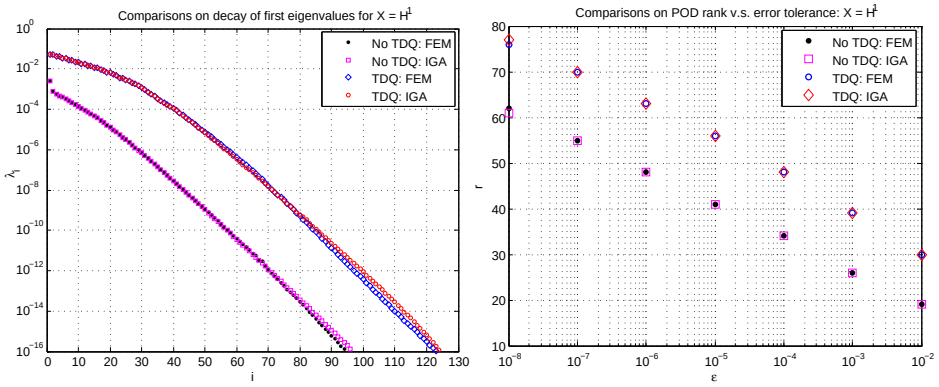

(a) (b)

Fig. 8 Comparisons of IGA-θ-POD and FEM-θ-POD Galerkin methods with $k_m = 1$, $X = H^1(\Omega)$ and $N_x = 16,641$ for Example 5.2: (a) decay of first eigenvalues of correlation matrix obtained with/without TDQ and (b) POD rank r vs. ε.

Table 2 Comparisons on errors $\mathscr{E}_{L^2}^{s,r}$ of POD-Galerkin solutions with respect to snapshots for Example 5.1: $X = H^1(\Omega)$.

ε	FEM	IGA $k_{\rm m}=0$	IGA $k_{\rm m}=1$	FEM	IGA $k_{\rm m}=0$	IGA $k_{\rm m}=1$
	N_x 1,233	N_x 1,173	N_x 1,144	N_x 4,801	N_x 4,141	N_x 4,116
No TDQ						
10^{-6}	1.32e-4	1.28e-4	1.27e-4	1.28e-4	1.27e-4	1.27e-4
10^{-8}	1.61e-5	6.58e-6	6.72e-6	8.78e-6	6.70e-6	6.71e-6
10^{-10}	1.10e-5	3.94e-7	2.77e-7	9.14e-6	2.71e-7	2.69e-7
10^{-12}	8.90e-6	1.56e-7	2.55e-8	7.72e-6	2.56e-8	9.05e-9
TDQ						
10^{-6}	2.95e-5	1.02e-5	1.00e-5	1.91e-5	9.98e-6	9.97e-6
10^{-8}	1.27e-5	1.16e-6	4.70e-7	1.02e-5	4.91e-7	4.05e-7
10^{-10}	9.08e-6	2.43e-7	2.37e-7	7.88e-6	8.96e-8	1.93e-8
10^{-12}	8.87e-6	1.73e-8	3.30e-8	7.76e-6	2.77e-8	1.53e-8

In the geometrical representation of Ω, both B-splines for IGA and uniform triangular elements for FEM allow an exact representation. In Fig. 7, we see that the IGA-θ-POD Galerkin solution is visually in agreement with the exact solution. In Table 4, with the same ndofs, snapshots obtained by IGA are more accurate than those obtained by FEM in L^2- and H^1- norms due to the smoothness of the B-splines basis functions used. Moreover, IGA is still more accurate than FEM even if much less ndofs are used. For both the cases with and without TDQ, we find from Fig. 8 (a) that POD eigenvalues of IGA cases decay nearly at the same rate as thoses of FEM cases as the eigenvalue index i increases. Therefore, POD ranks of the two methods are nearly the same for a prescribed threshold value of ε as shown in Fig. 8 (b). In Table 5, we see that the accuracy of POD-Galerkin solutions increases as ε decreases for both of FEM and IGA cases. Furthermore, IGA-θ-POD Galerkin solutions are more accurate than FEM-θ-POD Galerkin solutions when the same values of ε are used. The above comparisons show that although the spectral analysis for the generation of the POD basis associated to FEM and IGA are qualitatively and quantitatively very similar, the accuracy of the IGA-θ-POD solution is significantly higher than the one of the FEM-θ-POD solution. This advantage is mainly related to the use of high order continuous basis functions for the approximation of smooth solutions.

Table 3 Comparisons on effects of ε on POD truncation errors for Example 5.1: ndofs 4,801, 4,141 and 4,116 for FEM, IGA $k_{\rm m}=0$, and IGA $k_{\rm m}=1$, respectively.

ε	No TDQ			TDQ		
	FEM	IGA $k_{\rm m}=0$	IGA $k_{\rm m}=1$	FEM	IGA $k_{\rm m}=0$	IGA $k_{\rm m}=1$
$\sum_{i=r+1}^{\ell_d}\tilde{\lambda}_i$ $(X=H^1)$						
10^{-6}	1.03e-07	1.03e-07	1.03e-07	7.85e-08	6.96e-08	7.18e-08
10^{-8}	3.83e-10	3.19e-10	3.08e-10	5.84e-10	5.40e-10	2.60e-10
10^{-10}	8.83e-12	7.48e-13	7.99e-13	8.91e-12	4.61e-12	1.47e-12
10^{-12}	6.64e-14	1.82e-14	1.52e-15	4.16e-14	7.94e-14	5.99e-14
$\nu_1\sum_{i=r+1}^{\ell_d}\hat{\lambda}_i$ $(X=L^2)$						
10^{-6}	1.28e-07	1.26e-07	1.27e-07	2.04e-06	1.83e-06	1.66e-06
10^{-8}	8.86e-10	7.13e-10	7.05e-10	5.93e-07	3.09e-07	1.55e-08
10^{-10}	1.63e-10	7.13e-10	7.05e-10	1.24e-08	5.29e-09	1.72e-09
10^{-12}	2.15e-11	5.19e-12	2.04e-12	3.22e-10	3.99e-11	2.79e-11

Table 4 Comparisons between IGA and FEM on errors of truth approximations for Example 2.

$\mathscr{E}_Z$	$N_x=4,225$		$N_x=16,641$	
	FEM	IGA	FEM	IGA
$\mathscr{E}_{L^2}$	7.93e-4	5.18e-5	1.21e-4	8.91e-6
$\mathscr{E}_{H^1}$	2.35e-1	2.03e-2	6.67e-2	4.54e-3

Table 5 Comparisons on errors $\mathscr{E}_{r,Z}$ of POD-Galerkin solutions for Example 5.2: $N_x=16,641$.

ε	$X=H^1$				$X=L^2$			
	No TDQ		TDQ		No TDQ		TDQ	
	FEM	IGA	FEM	IGA	FEM	IGA	FEM	IGA
$\mathscr{E}_{r,L^2}$								
10^{-3}	6.99e-4	6.87e-4	1.87e-3	1.71e-3	9.63e-3	9.63e-3	1.59e-3	1.57e-3
10^{-4}	1.99e-4	1.53e-4	1.26e-4	4.74e-5	3.09e-3	3.09e-3	2.11e-4	1.77e-4
10^{-5}	1.29e-4	4.15e-5	1.21e-4	1.00e-5	1.01e-3	1.00e-3	1.25e-4	3.42e-5
10^{-6}	1.21e-4	1.46e-5	1.21e-4	9.10e-6	3.48e-4	3.26e-4	1.21e-4	1.23e-5
10^{-7}	1.21e-4	8.99e-6	1.21e-4	8.91e-6	1.26e-4	3.00e-5	1.21e-4	8.93e-6
$\mathscr{E}_{r,H^1}$								
10^{-3}	1.04e-1	8.12e-2	3.11e-1	2.61e-1	6.01e-1	6.00e-1	1.86e-1	1.76e-1
10^{-4}	7.08e-2	2.35e-2	6.71e-2	9.59e-3	2.73e-1	2.67e-1	7.16e-2	2.62e-2
10^{-5}	6.71e-2	7.41e-3	6.67e-2	4.66e-3	1.28e-1	1.11e-1	6.70e-2	7.62e-3
10^{-6}	6.68e-2	5.15e-3	6.67e-2	4.70e-3	7.95e-2	4.42e-2	6.67e-2	4.89e-3
10^{-7}	6.67e-2	4.61e-3	6.67e-2	4.54e-3	6.87e-2	1.75e-2	6.67e-2	4.58e-3

6 Conclusions

We have used IGA for the spatial approximation of snapshots for POD in model order reduction of linear parabolic PDEs, which may be thought as the simpliest model of parameterized PDEs. We split the error of the POD Galerkin solution into two parts and propose a fully IGA-θ-POD Galerkin scheme. We analyze the stability and convergence of the scheme by *a priori* error estimates. Numerical experiments are performed by comparing the IGA-θ-POD Galerkin scheme with the FEM-θ-POD Galerkin method. The comparisons have shown promising advantages of IGA when used as spatial truth approximation both with respect

to the "exact" geometrical representation of computational domains of practical interest and the use of smooth basis functions allowed by B-splines and NURBS.

7 Acknowledgements

The authors acknowledge Dr. Peng Chen and Dr. Toni Lassila for helpful discussions on model order reduction and Prof. Fabio Nobile for insights on error estimates. The help of Federico Negri with the library `MLife` developed by Prof. Fausto Saleri is acknowledged. The use of the IGA library `GeoPDEs` is also acknowledged. The third author greatly appreciates the warm hospitality of Prof. Quarteroni and other group members throughout his visit as a postdoctoral researcher at CMCS-MATHICSE-EPFL.

References

1. D. Amsallem, J. Cortial, K. Carlberg, C. Farhat, A method for interpolating on manifolds structural dynamics reduced-order models, Internat. J. Numer. Methods Engrg. 80 (2009) 1241-1258.
2. Y. Bazilevs, L. Beirão de Veiga, J.A. Cottrell, T.J.R. Hughes, G. Sangalli, Isogeometric analysis: approximation, stability and error estimates for *h*-refined meshes, Math. Models Methods Appl. Sci. 16 (2006) 1031-1090.
3. Y. Bazilevs, V.M. Calo, T.J.R. Hughes, Y. Zhang. Isogeometric fluid-structure interaction: theory, algorithms, and computations, Comput. Mech. 43 (2008) 3-37.
4. L. Beirão de Veiga, A. Buffa, J. Rivas, G. Sangalli, Some estimates for *h*-*p*-*k*-refinement in isogeometric analysis, Numer. Math. 118 (2011) 271-305.
5. G. Berkooz, P. Holmes, and J.L. Lumley, The proper orthogonal decomposition in the analysis of turbulent flows, Annu. Rev. Fluid Mech. 25 (1993) 539-575.
6. A. Buffa, G. Sangalli, R. Vázquez, Isogeometric analysis in electromagnetics: B-splines approximation, J. Comput. Phys. 199 (2010) 1143-1152.
7. D. Chapelle, A. Gariah, J. Sainte-Marie, Galerkin approximation with proper orthogonal decomposition: new error estimates and illustrative examples, ESAIM Math. Model. Numer. Anal. 46 (2012) 731-757.
8. S Chaturantabut, D.C. Sorensen, Nonlinear model reduction via discrete empirical interpolation, SIAM J. Sci. Comput. 32 (2010) 2737-2764.
9. J.A. Cottrell, T.J.R. Hughes, Y. Bazilevs, Isogeometric Analysis: Toward Integration of CAD and FEA. John Wiley & Sons, 2009.
10. J.A. Cottrell, T.J.R. Hughes, A. Reali, Studies of refinement and continuity in Isogeometric structural analysis, Comput. Methods Appl. Mech. Engrg. 196 (2007) 4160-4183.
11. R. Dautray, J.L. Lions, Mathematical Analysis and Numerical Methods for Science and Technology, in Evolution Problems I, vol. 5, Springer-Verlag, Berlin, 1992.
12. L. Dedè, M.J. Borden, T.J.R. Hughes, Isogeometric analysis for topology optimization with a phase field model, Arch. Comput. Methods Eng. 19 (2012) 427-465.
13. L. Dedè, C. Jäggli, A. Quarteroni, Isogeometric numerical dispersion analysis for elastic wave propagation, Comput. Methods Appl. Mech. Engrg. 284 (2015) 320-348.
14. L. Dedè, H.A.F.A. Santos, B-spline goal-oriented error estimators for geometrically nonlinear rods, Comput. Mech. 49 (2012) 35-52.
15. J.A. Evans, Y. Bazilevs, I. Babuška, T.J.R. Hughes, *n*-Widths, sup-infs, and optimality ratios for the *k*-version of the isogeometric finite element method, Comput. Methods Appl. Mech. Engrg. 198 (2009) 1726-1741.
16. C. de Falco, A. Reali, R. Vàzquez. GeoPDEs: a research tool for isogeometric analysis of PDEs, Adv. Eng. Softw. 42 (2011) 1020-1034.
17. P. Galàn del Sastre, R. Bermejo, Error estimates of proper orthogonal decomposition eigenvectors and Galerkin projection for a general dynamical system arising in fluid models, Numer. Math. 110 (2008) 49-81.
18. M.D. Gunzburger, J. Peterson, J.N. Shadid, Reduced-order modeling of time-dependent PDEs with multiple parameters in the boundary data, Comput. Methods Appl. Mech. Engrg. 196 (2007) 1030-1047.
19. T. Henri, J.P. Yvon, Stability of the POD and convergence of the POD Galerkin method for parabolic problems, IRMAR No 02-40, 2002.

20. T. Henri, J.P. Yvon, Convergence estimates of POD-Galerkin methods for parabolic problems, System Modeling and Optimization, IFIP International Federation for Information Processing Volume 166, 2005, pp 295-306.
21. P. Holmes, J.L. Lumley, G. Berkooz, Turbulence, Coherent Structures, Dynamical Systems and Symmetry, Cambridge Univ. Press, New York, 1996.
22. T.J.R. Hughes, J. Cottrell, Y. Bazilevs, Isogeometric analysis: CAD, finite elements, NURBS, exact geometry, and mesh refinement, Comput. Methods Appl. Mech. Engrg. 194 (2005) 4135-4195.
23. T.J.R. Hughes, J.A. Evans, A. Reali, Finite element and NURBS approximations of eigenvalue, boundary-value, and initial-value problems, Comput. Methods Appl. Mech. Engrg. 272 (2014) 290-320.
24. T. Iliescu, Z. Wang, Variational multiscale proper orthogonal decomposition: convection dominated convection-diffusion-reaction equations, Math. Comp. 82 (2013) 1357-1378.
25. T. Iliescu, Z. Wang, Are the snapshot difference quotients needed in the proper orthogonal decomposition? SIAM J. Sci. Comput. 36 (2014) A1221-A1250.
26. K. Kunisch, S. Volkwein, Control of the Burgers equation by a reduced-order approach using proper orthogonal decomposition, J. Optim. Theory Appl. 102 (1999) 345-371.
27. K. Kunisch, S. Volkwein, Galerkin proper orthogonal decomposition methods for parabolic problems, Numer. Math. 90 (2001) 117-148.
28. K. Kunisch, S. Volkwein, Galerkin proper orthogonal decomposition methods for a general equation in fluid dynamics, SIAM J. Numer Anal. 40 (2002) 492-515.
29. T. Lassila, A. Manzoni, A. Quarteroni, G. Rozza, Model order reduction in fluid dynamics: challenges and perspectives, Reduced Order Methods for Modeling and Computational Reduction, vol. 9, Springer Milano, MS&A Series, (2013) 235-273.
30. O. Lass, S. Volkwein, POD Galerkin schemes for nonlinear-parabolic systems, SIAM J. Sci Comp. 35 (2013) A1271-1298.
31. Z. Luo, J. Chen, I.M. Navon, X. Yang, Mixed finite element formulation and error estimates based on proper orthogonal decomposition for the nonstationary Navier-Stokes equations, SIAM. J. Numer. Anal. 47 (2008) 1-19.
32. Z. Luo, Z. Xie, Y. Shang, J. Chen, A reduced finite volume element formulation and numerical simulations based on POD for parabolic equations, J. Comput. Appl. Math. 235 (2011) 2098-2111.
33. L. Piegl, W. Tiller, The NURBS book, Springer-Verlag, New York, 1997.
34. A. Quarteroni, G. Rozza, A. Manzoni, Certified reduced basis approximation for parametrized partial differential equations and applications, J. Math. Ind. 1 (2011) 1-44.
35. A. Quarteroni, A. Valli, Numerical approximation of partial differential problems, Springer-Verlag, Berlin, 1997.
36. M. Rathinam, L.R. Petzold, A new look at proper orthogonal decomposition, SIAM J. Numer. Anal. 41 (2003) 1893-1925.
37. C.W. Rowley, Model reduction for fluids, using balanced proper orthogonal decomposition, Int. J. Bifurcation and Chaos, 15 (2005) 997-1013.
38. D. Schillinger, L. Dedè, M.A. Scott, J.A. Evans, M.J. Borden, E. Rank, T.J.R. Hughes, An Isogeometric design-through-analysis methodology based on adaptive hierarchical refinement of NURBS, immersed boundary methods, and T-spline CAD surfaces, Comput. Methods Appl. Mech. Engrg. 249-252 (2012) 116-150.
39. A. Schmidt, A. Potschka, S. Krkel, H.G. Bock, Derivative-extended POD reduced-order modeling for parameter estimation, SIAM J. Sci. Comput. 35 (2013) A2696-A2717.
40. J.R. Singler, Balanced POD for model reduction of linear PDE systems: convergence theory, Numer. Math. 121 (2012) 127-164.
41. J.R. Singler, New POD error expressions, error bounds, and asymptotic results for reduced order models of parabolic PDEs, SIAM J. Numer. Anal. 52 (2014) 852-876.
42. A. Tagliabue, L. Dedè, A. Quarteroni, Isogeometric analysis and error estimates for high order partial differential equations in fluid dynamics, Comput. & Fluids 102 (2014) 277-303.
43. V. Thomée, Galerkin Finite Element Methods for Parabolic Problems, Berlin: Springer, 1997.
44. S. Volkwein, Proper orthogonal decomposition: theory and reduced-order modelling, Lecture Notes, Universität Konstanz, 2013.
45. K. Willcox, J. Peraire, Balanced model reduction via the proper orthogonal decomposition, AIAA 40 (2002) 2323-2330.

MOX Technical Reports, last issues

Dipartimento di Matematica "F. Brioschi",
Politecnico di Milano, Via Bonardi 9 - 20133 Milano (Italy)

51/2014 Dassi, F.; Perotto, S.; Formaggia, L.
A priori anisotropic mesh adaptation on implicitly defined surfaces

52/2014 Dede , L..; Quarteroni, A.; S. Zhu, S.
Isogeometric analysis and proper orthogonal decomposition for parabolic problems

50/2014 Bartezzaghi, A.; Cremonesi, M.; Parolini, N.; Perego, U.
An explicit dynamics GPU structural solver for thin shell finite elements

49/2014 D. Bonomi, C. Vergara, E. Faggiano, M. Stevanella, C. Conti, A. Redaelli, G. Puppini et al
Influence of the aortic valve leaflets on the fluid-dynamics in aorta in presence of a normally functioning bicuspid valve

48/2014 Penta, R; Ambrosi, D; Shipley, R.
Effective governing equations for poroelastic growing media

47/2014 Penta, R; Ambrosi, D; Quarteroni, A.
Multiscale homogenization for fluid and drug transport in vascularized malignant tissues

46/2014 Penta, R; Ambrosi, D.
The role of the microvascular tortuosity in tumor transport phenomena

45/2014 Pezzuto, S.; Ambrosi,D.; Quarteroni, A.
An orthotropic active-strain model for the myocardium mechanics and its numerical approximation

44/2014 Pezzuto, S.; Ambrosi,D.
Active contraction of the cardiac ventricle and distortion of the microstructural architecture

43/2014 Brugiapaglia, S.; Micheletti, S.; Perotto, S.
Compressed solving: a numerical approximation technique for PDEs based on compressed sensing